eLife

Reviewed Preprint
v1 • April 30, 2026
Not revised

For correspondence:
hm069@foxmail.com
sguang@ustc.edu.cn
fengxuezhu@ahmu.edu.cn

* Lead contact.

Competing interests: No competing interests declared

Funding: See page 25

Reviewing editor: Sylvia Lee, Cornell University, United States

Identification of a somatic H3K23me3 methyltransferase SET-19 in *C. elegans*

Mingjing Xu[1], Zixue Fan[2], Chaoyue Yan[1], Xiangyang Chen[1], Xinya Huang[1], Chengming Zhu[2], Minjie Hong[1], Jiewei Cheng[1], Xinhao Hou[1], Shuju Li[1], Mengfeng Li[1], Yunyu Shi[1], Meng Huang[3] ✉, Shouhong Guang[1,*] ✉, Xuezhu Feng[2] ✉

[1]Department of Obstetrics and Gynecology, The First Affiliated Hospital of USTC, The USTC RNA Institute, Ministry of Education Key Laboratory for Membraneless Organelles & Cellular Dynamics, Hefei National Research Center for Physical Sciences at the Microscale, Center for Advanced Interdisciplinary Science and Biomedicine of IHM, School of Life Sciences, Division of Life Sciences and Medicine, University of Science and Technology of China, Hefei, China • [2]School of Basic Medical Sciences, Anhui Medical University, Hefei, China • [3]School of Food and Biological Engineering, Hefei University of Technology, Hefei, China

eLife Assessment

This study provides **fundamental** insight by identifying C. elegans SET-19 as a key enzyme that deposits H3K23me to somatic chromatin. The evidence is **compelling**, using a broad and modern toolkit of biochemical, genetic, and genome-wide analyses that consistently support the main claims. The significance of the study is further strengthened by the fact that H3K23me is an understudied histone modification, which is also conserved in mammals.

https://doi.org/10.7554/eLife.111326.1.sa3

Abstract

Histone methylation plays essential roles in modulating chromatin organization and gene expression. H3K23 methylation is a conserved histone modification, yet its biological roles and the enzymes responsible for its deposition remain poorly understood. Here, we show that the loss of *set-19* leads to a pronounced reduction in H3K23 methylation in *C. elegans*, as revealed by quantitative mass spectrometry, western blotting, and immunofluorescence staining. In vitro biochemical assays show that recombinant SET-19 proteins purified from *E. coli* directly catalyze H3K23 methylation. Genome-wide chromatin immunoprecipitation assays reveal that H3K23me3 is enriched at heterochromatic regions and that loss of *set-19* alters H3K23me3 levels, accompanied by derepression of gene expression. Genetic analyses indicate that SET-19 is dispensable for both germline and somatic RNAi as well as transgenerational epigenetic inheritance of RNAi. SET-19 is predominantly expressed in somatic cells and specifically mediates H3K23me3 deposition in somatic tissues. The loss of *set-19* causes a developmental delay without affecting fertility. Together, our results identify SET-19 as a somatic H3K23 methyltransferase and link H3K23me3 to gene repression in *C. elegans*.

Introduction

The nucleosome, composed of DNA wrapped around histone proteins (H2A, H2B, H3, and H4), is the fundamental structural unit of chromatin. Post-translational modifications (PTMs), such as methylation, acetylation, and phosphorylation, occur on both histone tails and core regions [1]. Histone modifications function as epigenetic marks that regulate chromatin organization and stability, as well as DNA replication, repair, and transcription.

Chromatin is broadly divided into euchromatin and heterochromatin, which differ in their degrees of compaction and transcriptional activity. Histone PTMs such as acetylation, H3K4me3, and H3K36me3 are typically enriched in transcriptionally active euchromatic regions and are associated with gene activation. In contrast, repressive marks including H3K9me3 and H3K27me3 are preferentially enriched in transcriptionally silent heterochromatic regions. The distinct genomic distributions of these modifications reflect their diverse regulatory functions, and the dynamic regulation of these marks across tissues and developmental stages contributes to cell fate determination, fertility, development, and epigenetic inheritance [2-6].

Histone PTMs are dynamically regulated by specific writers, readers, and erasers, which establish, recognize, and remove these modifications, respectively [1,7]. Writers responsible for histone methylation are histone methyltransferases (HMTs), which catalyze the methylation of lysine (K) and arginine (R) residues on histone proteins. Lysine residues can be mono-, di-, or trimethylated by lysine methyltransferases (KMTs), whereas arginine residues can be mono- or dimethylated by arginine methyltransferases (RMTs) [8]. Most KMTs harbor a conserved SET domain that confers catalytic activity and substrate specificity [7,9-11].

Histone H3 lysine 23 methylation (H3K23me) is widely conserved across eukaryotic species [12-24]. In organisms including *Tetrahymena*, *C. elegans*, and mammals, evidence from immunostaining, chromatin immunoprecipitation (ChIP)-based analyses, and binding studies with HP1 family proteins supports an association of H3K23 methylation with heterochromatic regions [14,15,17,18,20,21,24-26]. In *Tetrahymena*, the loss of the H3K23 methyltransferase Ezl3p leads to aberrant targeting of meiosis-induced DNA double-strand breaks to heterochromatin and compromises progeny viability [17]. In *C. elegans*, H3K23me3 shares genomic features with classical repressive marks such as H3K9me3 and H3K27me3 and is also associated with transgenerational epigenetic silencing and accumulation at RNAi target loci [25-30]. The loss of the corresponding histone methyltransferases for H3K9me3 and H3K27me3 results in varying degrees of RNAi defects [30-33]. Two methyltransferases, SET-32 and SET-21, have been reported to contribute to H3K23 methylation [25,26], but no obvious global reduction in H3K23 methylation has been detected in vivo upon loss of either enzyme. Nevertheless, the enzymatic basis, tissue-specific regulation, and biological functions of H3K23 methylation remain far less well characterized than those of other histone methylation marks. The *C. elegans* genome encodes 38 SET domain-containing KMTs [34-45], many of which remain functionally uncharacterized. Our previous work showed that the loss of *set-19* leads to a significant reduction in H3K23me3 levels in vivo [46], implicating SET-19 as a candidate H3K23 methyltransferase.

In this work, we investigated the role of SET-19 in H3K23 methylation in *C. elegans* and showed that SET-19 functions as a somatic H3K23 methyltransferase required for H3K23me3 methylation in vitro and in vivo. This work provides insights into how H3K23 methylation is established and supports the idea that distinct methyltransferases may function in different tissues or cell types to promote proper development.

Results

SET-19 is required for H3K23 methylation in *C. elegans*

In *C. elegans*, the biological functions of many SET domain-containing methyltransferases remain poorly understood [25,26,34-44]. SET-19 harbors a conserved SET domain (Fig. 1a). Our previous work showed that the *set-19(ok1813)* mutant exhibited reduced levels of H3K23me2 and H3K23me3, as detected by western blotting [46]. However, the role of SET-19 in H3K23 methylation required further validation.

To assess the impact of *set-19* loss on histone H3 methylation, we quantified global H3 methylation levels in the *set-19(ok1813)* mutant by mass spectrometry at the L3–L4 larval and embryonic stages. No significant changes were observed in the methylation levels of H3K4, H3K9, H3K27, or H3K36 compared with those in wild-type animals (Fig. 1b–d and Fig. S1). In contrast, H3K23 methylation was markedly reduced in the *set-19(ok1813)* mutant (Fig. 1b–d and Fig. S1). Specifically, H3K23me3 levels decreased from approximately 33.8% to 5.4% at the larval stage and

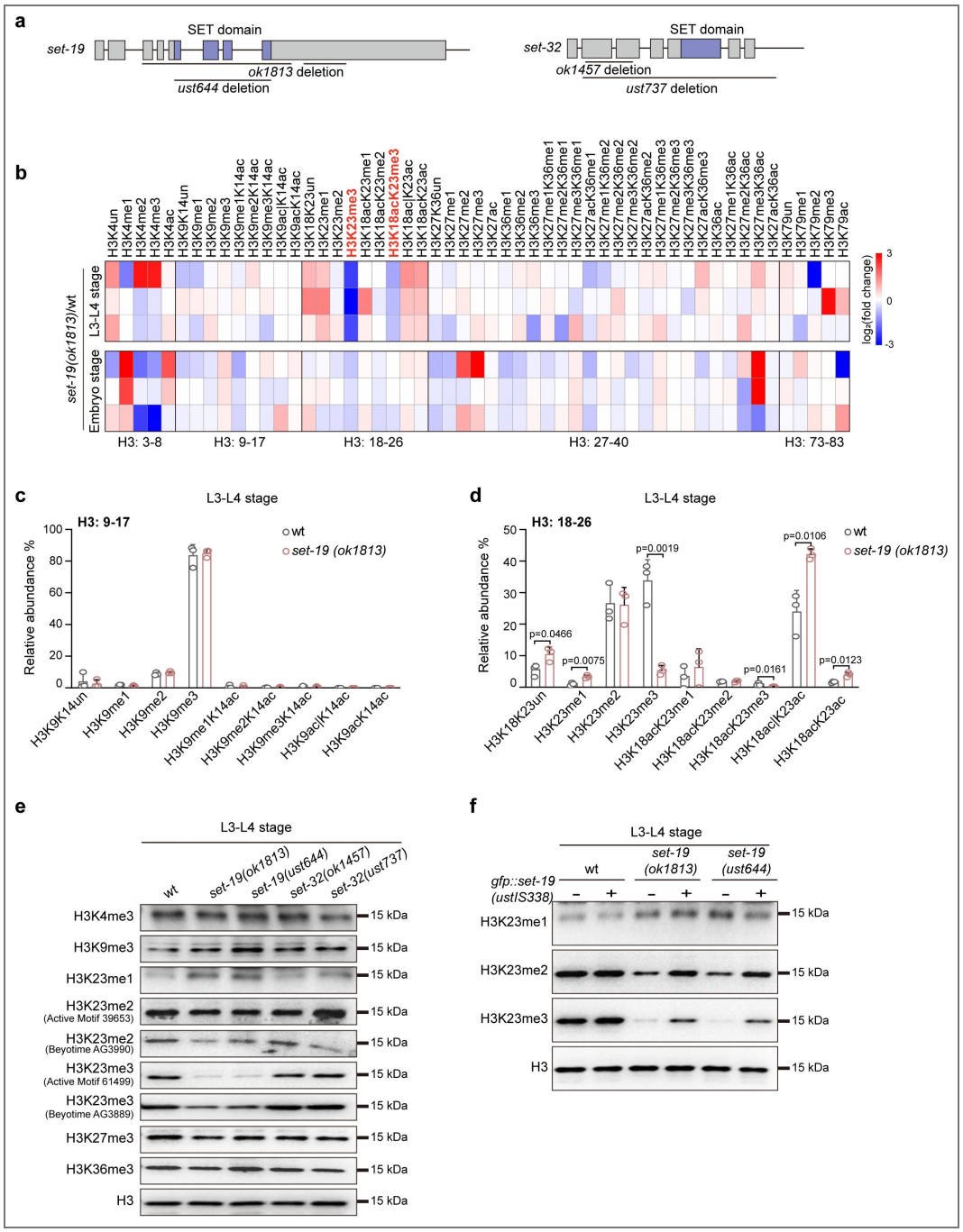

Fig. 1. Loss of SET-19 leads to a marked reduction of H3K23me3.

a, Schematic representation of the *set-19* and *set-32* genes. The *set-19(ok1813)* allele contains two large deletions and likely functions as a null allele. The *set-19(ust644)* allele carries a precise deletion of the SET domain, and the open reading frame is retained. The *set-32(ok1457)* allele contains a deletion that does not disrupt the open reading frame (ORF), whereas *set-32(ust737)* harbors a large deletion and likely functions as a null allele. SET domains are indicated in purple. **b,** Heatmap showing relative abundances of histone H3 post-translational modifications (PTMs) measured by mass spectrometry. Values represent $\log_2$(fold change) in *set-19(ok1813)* mutants relative to wild-type (wt) animals for each biological replicate. **c, d,** Quantification of H3(9–17) and H3(18–26) methylation states in wild-type and *set-19(ok1813)* animals at the indicated developmental stages. Methylation levels are shown as relative abundances, calculated as the area under the curve (AUC) of each modified peptide divided by the sum of all detected forms of that peptide. Differences without indicated p values are not statistically significant (two-tailed t test, $p < 0.05$). $N = 3$ biological replicates. **e,** Western blotting analysis of global H3 methylation levels in L3–L4 stage worms of the indicated genotypes. **f,** Western blotting analysis of H3K23me1/2/3 levels in L3–L4 worms. The *fib-1p::gfp::set-19(ustIS338)* transgene was used for rescue.

from 10% to 8% at the embryonic stage (Fig. 1d and Fig. S1f). Mass spectrometry revealed no significant change in H3K23me2, whereas H3K23me1 levels were slightly increased at the L3–L4 larval stage (Fig. 1d), and a slight reduction of H3K9me2 was detected in embryos (Fig. S1e).

To further confirm the role of SET-19, we generated an independent *set-19* allele using CRISPR/Cas9-mediated genome editing. This allele, *set-19(ust644)*, precisely deletes the SET domain without disrupting the open reading frame (ORF) (Fig. 1a). Western blotting analysis revealed that both *set-19(ok1813)* and *set-19(ust644)* mutants exhibited a pronounced reduction in H3K23me3 and a detectable decrease in H3K23me2 at the larval stage (Fig. 1e and Fig. S2a). Two independent antibodies specific for H3K23me2 and H3K23me3, respectively, were used in the western blotting assays. Importantly, reintroduction of a GFP::SET-19 transgene (*fib-1p::gfp::set-19*, ustIS338) into the *set-19* mutant background restored H3K23me2 and H3K23me3 levels (Fig. 1f and Fig. S2b, c). Consistent with previous reports [25,26], the loss of *set-32* did not lead to a detectable reduction in H3K23 methylation in western blotting assays (Fig. 1e and Fig. S2a).

Together, these results indicate that SET-19 is required for H3K23 methylation, particularly H3K23me3 in *C. elegans*.

Recombinant SET-19 catalyzes histone H3K23 methylation in vitro

SET-19 contains a central SET domain and a nearby coiled-coil region, with intrinsically disordered regions (IDRs) at both the N- and C-termini (Fig. 2a). To test whether SET-19 is a bona fide methyltransferase, we performed in vitro histone methylation assays. Full-length SET-19 and SET-19 domain fragments were fused to GST, expressed in *E. coli*, and purified using glutathione beads. Although full-length SET-19 could not be successfully expressed in *E. coli* and was therefore excluded from subsequent analyses, we obtained purified GST-fused proteins corresponding to the SET domain alone (SET-19 SET; amino acids 37–318) and a fragment containing both the SET and coiled-coil domains (SET-19 SET+CC; amino acids 37–454) (Fig. 2a). SET-32 has previously been reported to exhibit H3K23 methyltransferase activity in vitro and was therefore included as a positive control [25]. Given the high evolutionary conservation of histone H3 and the conserved nature of lysine 23 across species (Fig. S3a), human histone H3 (Active Motif, #31294) was used as the methylation substrate. Purified GST-SET-19 fusion proteins or full-length GST-SET-32 were incubated with unmodified H3 in the presence of the methyl donor S-adenosylmethionine (SAM). The reaction products were analyzed by western blotting using a panel of antibodies recognizing distinct H3 methylation marks.

In the in vitro methylation assays, neither the SET-19 fragments nor full-length SET-32 induced detectable changes in H3K4me3, H3K9me3, H3K27me3, or H3K36me3 levels (Fig. 2b and Fig. S3b). In contrast, the SET-19 SET+CC fragment, but not the SET domain alone, induced a pronounced increase in H3K23me1, H3K23me2, and H3K23me3 signals (Fig. 2b and Fig. S3b), indicating that SET-19 specifically methylates H3K23 in vitro and that this activity requires sequences outside the SET domain, which likely helps the folding of the SET domain. SET-32 exhibited modest H3K23me1 methyltransferase activity, but did not appreciably catalyze H3K23me2 or H3K23me3 under the same conditions (Fig. 2b and Fig. S3b).

SET domain-containing methyltransferases differ not only in substrate specificity but also in their sensitivity to SAM concentration [39,47-50]. We then examined the enzymatic activities of GST-SET-19 SET+CC and full-length GST-SET-32 across a range of SAM concentrations. Increasing SAM levels enhanced H3K23me1/2/3 signals for both enzymes; however, SET-19 SET+CC consistently exhibited substantially higher catalytic activity than SET-32 (Fig. 2c and Fig. S3c). No methylation at other lysine residues, including H3K4, H3K9, H3K27, or H3K36, was detected under any of the tested conditions (Fig. 2c and Fig. S3c). These results indicate that although both SET-19 and SET-32 are capable of catalyzing H3K23 methylation in vitro, SET-19 shows markedly higher enzymatic activity, consistent with the western blotting analyses (Fig. 1e).

Notably, although SET-19 catalyzed mono-, di-, and trimethylation of H3K23 in vitro, both mass spectrometry and western blotting analyses revealed a predominant reduction in H3K23me3 upon loss of *set-19*. Together, these in vitro and in vivo data establish SET-19 as an H3K23

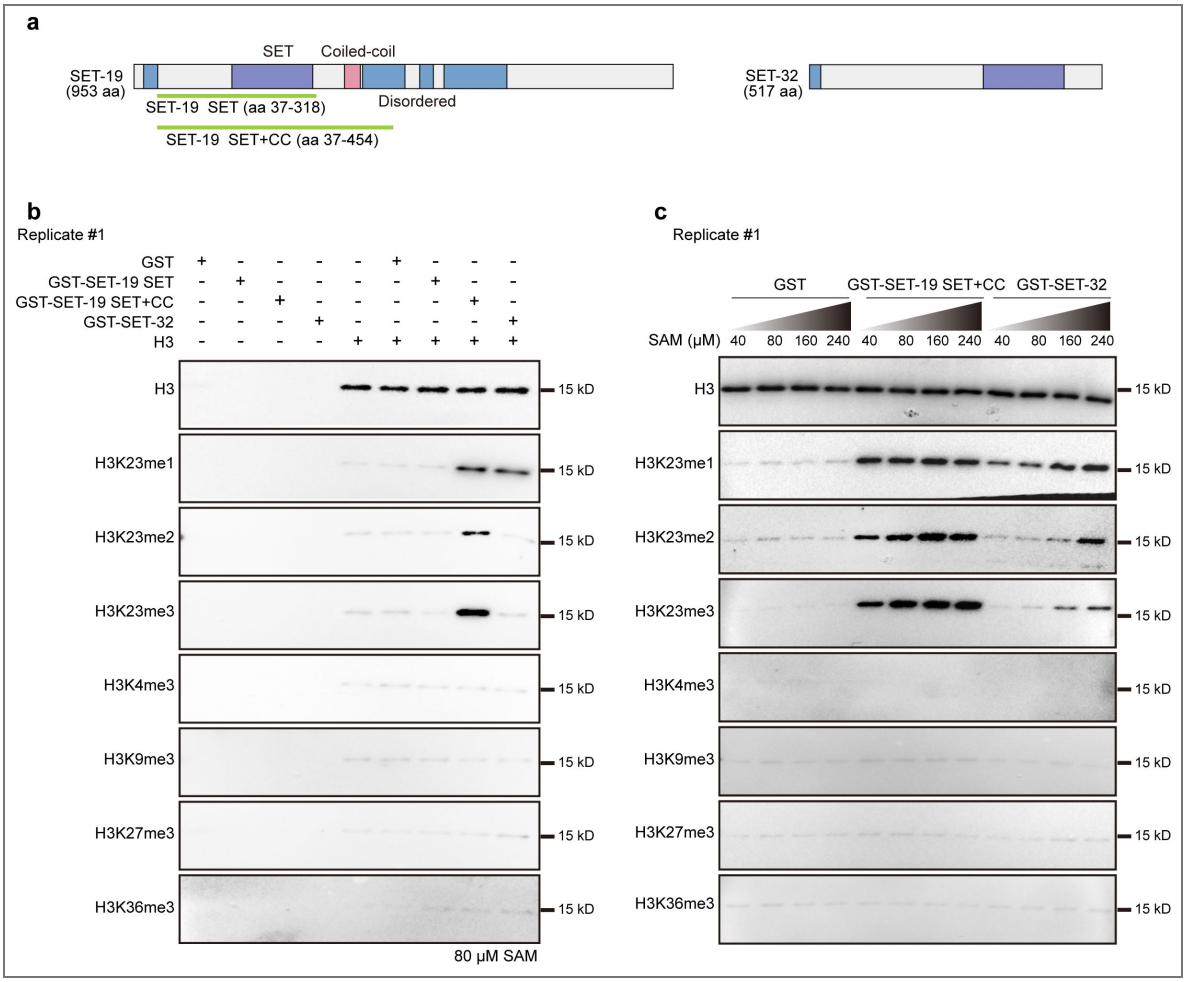

Fig. 2. SET-19 specifically catalyzes histone H3K23 methylation in vitro.

a, Schematic diagram of SET-19 and SET-32 proteins. Purple: SET domain, blue: disordered region, pink: coiled-coil region. Recombinant SET-19 SET or SET+CC fragments are shown in green. **b,** In vitro histone methyltransferase assays using GST-fused SET-19 SET or SET+CC fragments or full-length SET-32 incubated with histone H3 and 80 μM S-adenosylmethionine (SAM). Methylation was detected by western blotting. **c,** In vitro methylation assays performed as in (**b**) with increasing concentrations of SAM.

methyltransferase in *C. elegans* and indicate that SET-19 plays a prominent role in H3K23 trimethylation.

SET-19 is required for genomic H3K23me3 occupancy and gene repression

Previous studies using ChIP-seq and immunofluorescence staining have shown a strong association between H3K23 methylation (H3K23me2/3) and heterochromatin marks [17,18,20,21,24-26]. In *C. elegans*, the genome-wide distribution of H3K23me3 closely resembles those of H3K9me3 and H3K27me3 (Fig. S4a). *C. elegans* chromosomes are organized into broad domains, with active marks (H3K4me3 and H3K36me3) enriched in central regions and repressive marks (H3K9me1/2/3) enriched in distal arms [34,51-53]. Consistent with this chromosomal organization, H3K23me3-enriched regions were predominantly localized to chromosome arms (Fig. S4b). In addition, regions centered on H3K23me3 peaks show stronger enrichment of H3K9me3 and H3K27me3 than of the active marks H3K4me3 and H3K36me3 (Fig. 3a).

To examine whether SET-19 is required for H3K23me3 occupancy across the genome, we compared H3K23me3 ChIP-seq profiles between wild-type and *set-19* mutant animals. The loss of *set-19* led to a pronounced global reduction in H3K23me3 levels across the genome (Fig. 3b, c and Fig. S4c). Differential binding analysis using DiffBind [54] revealed that 55.4% of H3K23me3 peaks were significantly reduced in the *set-19* mutant relative to wild-type animals (Fig. S4d). Notably, residual H3K23me3 signals remained in the *set-19* mutant (Fig. 3b, c and Fig. S4c, d), suggesting additional H3K23 methyltransferases besides SET-19 may also contribute to H3K23 methylation.

H3K23me3 has been shown to be required for transcriptional repression of nuclear RNAi-targeted genes [25,26]. To investigate the contribution of SET-19-dependent H3K23me3 to gene regulation, we performed mRNA-seq analysis in wild-type N2 and *set-19* mutant animals. Genes were grouped into five categories based on their expression levels in wild-type N2 animals, and then H3K23me3 levels were quantified for each group. H3K23me3 levels showed a strong negative correlation with gene expression, with lowly expressed genes exhibiting higher H3K23me3 occupancy (Fig. 3d, e). Transcriptome analysis revealed that 520 genes were significantly upregulated and 130 genes were downregulated in the *set-19* mutant compared with wild-type animals (Fig. 3f). Importantly, the upregulated genes displayed reduced H3K23me3 levels in the *set-19* mutant (Fig. 3g), indicating that the loss of SET-19-dependent H3K23me3 is associated with transcriptional derepression.

Collectively, these results indicate that SET-19 is required for genomic H3K23me3 occupancy and is linked to transcriptional repression.

SET-19 is dispensable for feeding RNAi targeting both germline and somatic genes

H3K23me3 and the putative H3K23 methyltransferase SET-32 have previously been implicated in transgenerational epigenetic inheritance (TEI) [25,26,31,33,55]. We first tested whether SET-19 is required for feeding RNAi targeting several germline and somatic genes, including *pos-1*, *mex-3*, *dpy-11*, and *unc-15*. RNAi targeting *pos-1* or *mex-3* causes embryonic lethality and results in unhatched F1 embryos [56-58]. RNAi targeting *dpy-11* or *unc-15* induces dumpy and paralysis phenotypes, respectively [59-61]. However, neither *set-19* nor *set-32* mutants displayed detectable defects in these feeding RNAi responses (Fig. S5a–d). RDE-1 is an essential Argonaute protein required for feeding RNAi response [62]. As a control, *rde-1* mutants were completely resistant to feeding RNAi. To increase the sensitivity of feeding RNAi assays, we next used an enhanced RNAi background [60]. In *eri-1* mutants, RNAi targeting *dpy-11* resulted in a strongly enhanced dumpy phenotype in the progeny. RNAi targeting *lir-1* induced larval arrest, and targeting *dpy-13* induced a super dumpy phenotype [60,63,64]; both phenotypes were abolished by *nrde* mutation. However, the *eri-1;set-19* mutant remained fully competent for feeding RNAi against *dpy-11*, *lir-1*, and *dpy-13* (Fig. S5e–g).

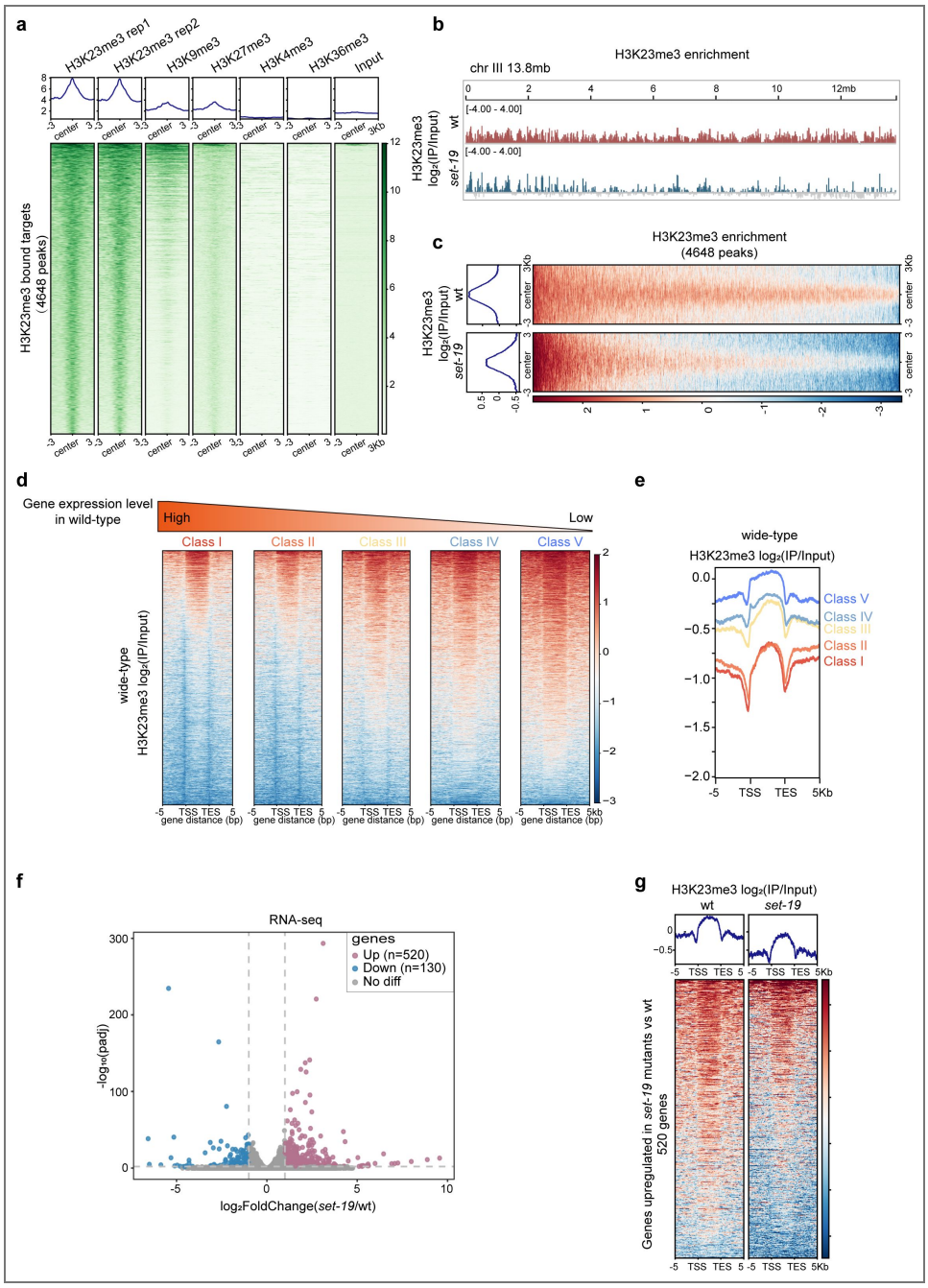

Fig. 3. SET-19 is required for genomic H3K23me3 occupancy and transcriptional repression.

a, Heatmaps showing ChIP-seq signal enrichment of heterochromatic marks (H3K9me3, H3K27me3) and euchromatic marks (H3K4me3, H3K36me3) centered on H3K23me3 peak summits. The average signal within ±3 kb regions is shown. **b,** Genome browser view of H3K23me3 ChIP-seq signals across chromosome III in wild-type and *set-19(ok1813)* animals. Mean $\log_2$ enrichment over input is shown (N = 2 biological replicates). **c,** Heatmaps comparing H3K23me3 profiles on H3K23me3 target regions in wild-type and *set-19(ok1813)* worms. Mean $\log_2$ enrichment over input within ±3 kb of peak summits is shown. **d,** Heatmaps of H3K23me3 enrichment across gene bodies in wild-type worms. Genes were grouped into quintiles based on RNA-seq expression levels; genes with zero expression were excluded. **e,** Average H3K23me3 profiles corresponding to the gene groups shown in (**d**). **f,** RNA-seq analysis of *set-19(ok1813)* relative to wild-type worms. Volcano plot showing $\log_2$FoldChange (*set-19*/wt) versus -$\log_{10}$(adjusted p value [padj]), calculated using DESeq2. Significantly upregulated and downregulated genes are highlighted (padj < 0.01; $|\log_2\text{FoldChange}| > 1$). N = 3 biological replicates. **g,** H3K23me3 enrichment [$\log_2$(IP/Input)] across gene bodies for genes upregulated in *set-19* mutants. Heatmaps showing a global reduction in the H3K23me3 signal in *set-19(ok1813)* relative to wild-type animals, with average enrichment profiles shown above.

We then asked whether SET-19 also participates in the transgenerational epigenetic inheritance of RNAi. We employed a germline-expressed *pie-1*$_p$*::h2b::gfp* reporter and performed feeding RNAi against *gfp* for one generation, after which animals were transferred to fresh plates without continued RNAi exposure. As expected, wild-type animals silenced *gfp* expression in the parental generation and maintained robust silencing in their F1 progeny. In *hrde-1*, *set-25*, and *set-32* mutants, the parental generation remained sensitive to feeding RNAi, but silencing inheritance was abolished in the F1 progeny (Fig. 4a, b). In contrast, *set-19* mutants retained effective *gfp* silencing in both the parental and F1 generations, comparable to that in control animals (Fig. 4a, b). Similarly, we tested whether SET-19 is required for the intergenerational inheritance of RNAi using a soma-expressed *sur-5p::gfp* reporter. Feeding dsRNA targeting *gfp* resulted in efficient silencing of GFP expression in both parental animals and F1 progeny in control animals (Fig. 4c). As expected, GFP expression was not silenced in the *rde-1* mutant, consistent with the essential role of RDE-1 in feeding RNAi responses. NRDE-3 is required for the intergenerational inheritance of RNAi targeting somatic genes [60]. In *nrde-3* mutants, the somatic *sur-5p::gfp* was silenced in the parental generation, but this silencing was abolished in the F1 progeny. In *set-19* and *set-32* mutants, *sur-5p::gfp* remained silenced in both parental and progeny generations (Fig. 4c, d).

Thus, these results suggest that SET-19 is dispensable for RNAi and its inheritance in *C. elegans*.

SET-19 is predominantly expressed in somatic cells and required for developmental timing

To explore the physiological roles of SET-19, we examined the development and reproduction of *set-19* mutants, but did not observe significant defects in brood size or hatch rate compared with wild-type animals (Fig. 5a, b). However, *set-19* mutants exhibited a modest developmental delay relative to wild-type animals (Fig. 5c).

Publicly available expression data from WormBase (version WS297) showed that *set-19* mRNA is more highly expressed in embryos than in larvae (Fig. 5d). To further examine cell type-specific expression, we analyzed published single-cell RNA-seq data from L2-stage larvae [65]. *set-19* expression was relatively enriched in intestinal cells and neurons (Fig. 5e).

To directly assess the expression and subcellular localization of SET-19, we generated an endogenous GFP-tagged SET-19 strain using CRISPR/Cas9-mediated genome editing. GFP::SET-19 was broadly expressed in somatic cells during both embryonic and larval stages and was predominantly localized to the nucleus (Fig. 5f–h). During embryogenesis, SET-19 expression was low in early embryos but markedly increased in late embryos (Fig. 5h). No detectable GFP::SET-19 signal was observed in germ cells (Fig. 5g). In contrast, SET-32 was highly expressed in germ cells, displayed both nuclear and cytoplasmic localization during larval stages, and was weakly expressed in embryos (Fig. S6a–c).

These results indicate that SET-19 is predominantly expressed in somatic cells and is largely excluded from the germline.

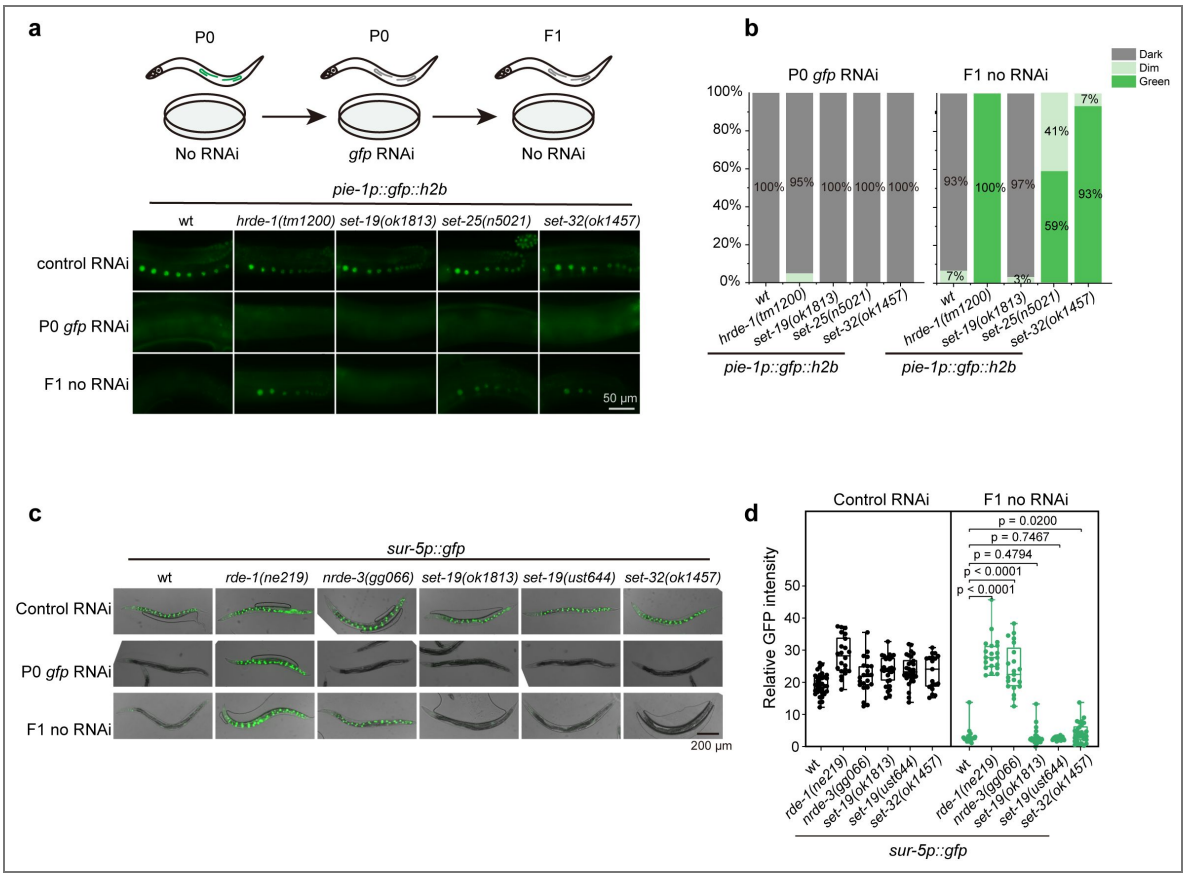

Fig. 4. SET-19 is dispensable for feeding RNAi and its inheritance.

a, Representative fluorescence images of animals expressing *pie-1*$_p$*::gfp::h2b* subjected to *gfp* RNAi or control treatment. F1 progeny were maintained on control bacteria without feeding RNAi. **b,** The percentages of the indicated P0 and F1 animals expressing GFP were quantified. At least 30 animals were scored per genotype and generation. **c,** Representative fluorescence images of animals expressing *sur-5p::gfp* following *gfp* RNAi treatment. **d,** Quantification of relative GFP fluorescence intensity for animals shown in (**c**). Data are presented as the mean ± SD (*N* = 3 biological replicates; n > 18 worms per genotype). Statistical significance was assessed using a two-tailed t test.

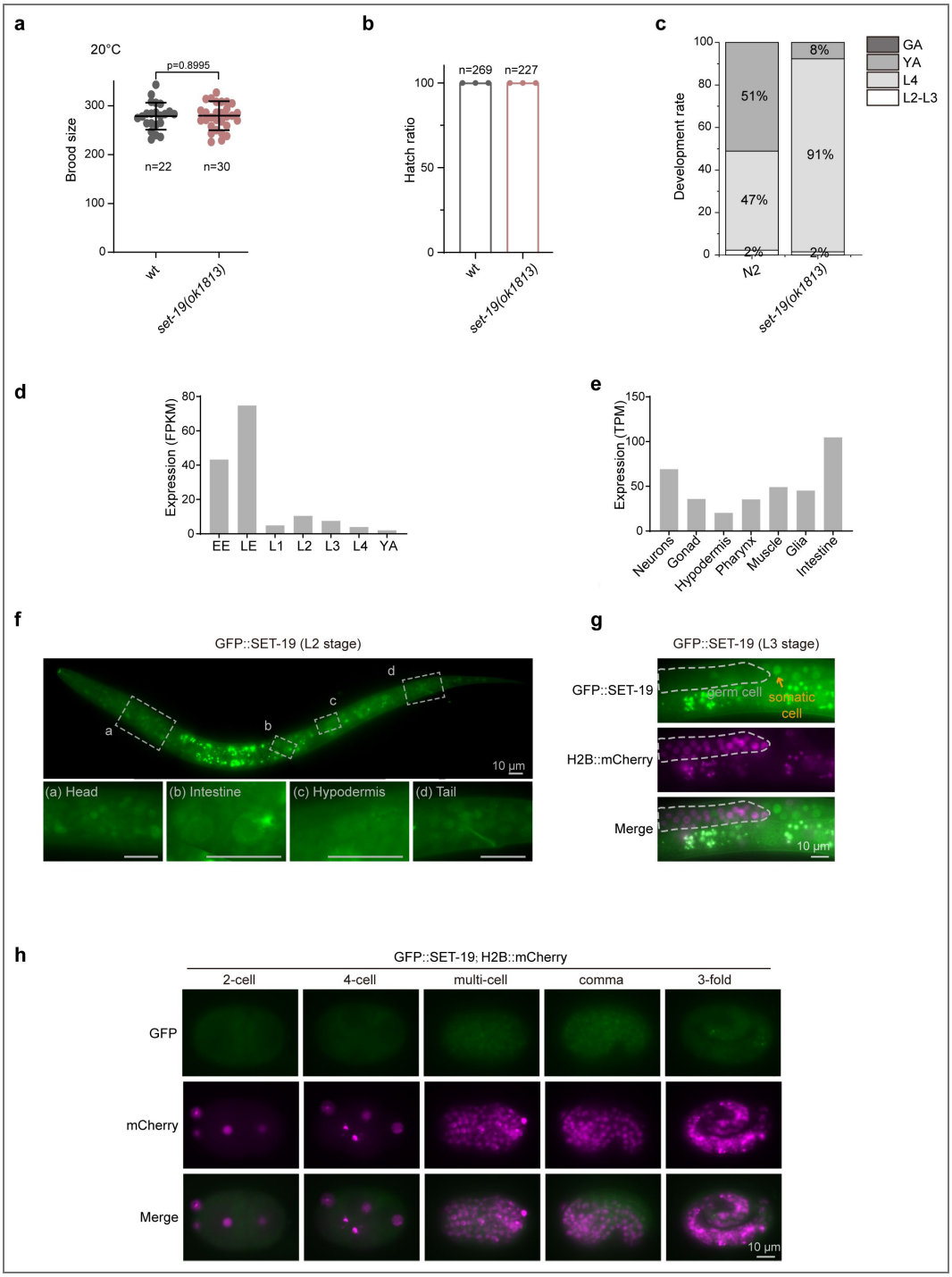

Fig. 5. SET-19 is expressed in somatic cells and required for developmental timing.

a, Brood size of the indicated genotypes maintained at 20°C. Individual L4 animals were transferred to fresh NGM plates, and total progeny were counted. **b,** Hatch rate of embryos laid by synchronized adult hermaphrodites at 20°C. The hatch rate was calculated as the ratio of hatched larvae to total embryos. **c,** Developmental progression of the indicated genotypes at 20°C (n > 50). **d,** The expression levels of *set-19* mRNA at different developmental stages. Data were downloaded from WormBase (version WS297). EE, early embryos; LE, late embryos; YA, young adults. **e,** The expression levels of *set-19* mRNA in different tissues at the L2 stage [65]. **f,** Fluorescence images of L2 animals expressing GFP::SET-19. **g,** Fluorescence images of L3 animals expressing GFP::SET-19 and H2B::mCherry. GFP::SET-19 shows enrichment in somatic cells. **h,** Subcellular localization of GFP::SET-19 and H2B::mCherry in embryos.

SET-19 conducts H3K23 trimethylation predominantly in somatic cells

To further examine the role of SET-19 in H3K23me3 in vivo, we performed immunofluorescence staining and assessed H3K23me3 levels across different developmental stages and tissues. In wild-type N2 animals, H3K23me3 signals were readily detected throughout development and were broadly distributed across tissues (Fig. 6a–d). Consistent with the somatic expression pattern of SET-19, the loss of *set-19* resulted in a pronounced reduction in H3K23me3 in somatic cells (Fig. 6a). However, no obvious reduction of H3K23me3 was observed in embryos (Fig. 6b). In young adult worms, the reduction in H3K23me3 was most prominent in intestinal cells (Fig. 6c), a tissue in which *set-19* expression is relatively enriched (Fig. 5e). Notably, H3K23me3 levels in germ cells remained largely unchanged in *set-19* mutants (Fig. 6d), consistent with the absence of detectable *set-19* expression in the germline (Fig. 5g).

For comparison, we analyzed H3K23me3 levels in *set-32* mutants. The loss of *set-32* resulted in no, if any, detectable reduction in H3K23me3 across tissues or developmental stages (Fig. 6a–d), suggesting that SET-32 is unlikely to act as the major H3K23me3 methyltransferase in *C. elegans*.

Together, these results support a major role for SET-19 in establishing H3K23me3 in somatic cells.

Discussion

H3K23me3 is a histone modification presented across multiple species, yet its mechanisms of deposition and biological functions have remained poorly defined. In this study, we identified SET-19 as an H3K23me3 methyltransferase through a combination of biochemical and in vivo approaches. We show that SET-19-dependent H3K23me3 is enriched at heterochromatin-associated regions and is associated with transcriptional repression. SET-19-dependent deposition of H3K23me3 occurs predominantly in somatic tissues in *C. elegans*. Collectively, these findings extend our understanding of how H3K23 methylation is established and suggest that its deposition is regulated in a tissue-specific manner.

Histone lysine methylation is generally catalyzed by SET domain-containing methyltransferases. The *C. elegans* genome encodes at least 38 SET domain-containing lysine methyltransferases, yet only a subset of them have been functionally characterized [35-44,66-69]. To date, efforts to identify the enzymes responsible for H3K23 methylation have been relatively limited. Candidate-based analyses assessed H3K23me2 by immunostaining in primordial germ cells and the adult germline, but failed to identify a bona fide KMT for germline H3K23me2 [18]. SET-32 was then shown to methylate H3K23 in vitro and to be required for nuclear RNAi-induced H3K23me3 in vivo [25,26]. Subsequently, the closely related methyltransferase SET-21 was also shown to possess H3K23 methyltransferase activity in vitro, predominantly generating H3K23me1 and H3K23me2. SET-32 and SET-21 are more strongly associated with the germline [26]. Yet single loss of *set-32* or *set-21* did not cause a noticeable reduction in overall H3K23 methylation. Here, we show that SET-19 functions as a new H3K23me3 methyltransferase that acts primarily in somatic tissues. Based on our findings together with previous reports, we therefore propose a working model in which SET-19 predominantly mediates H3K23me3 deposition in somatic cells, whereas germline H3K23 methylation may rely more heavily on SET-32 and SET-21 (Fig. 7).

Classical heterochromatin marks, such as H3K9 and H3K27 methylation, play essential roles in transcriptional repression, perinuclear anchoring of chromatin, genome stability, and RNAi-mediated gene silencing [27-30,70-72]. Previous studies linked H3K23me3, particularly SET-32-associated H3K23 methylation, to nuclear RNAi and transgenerational epigenetic inheritance [25,26,29,31,33,73]. Immunofluorescence staining shows that H3K23me3 forms discrete foci within the nucleus, resembling the nuclear distribution patterns reported for H3K9 and H3K27 methylation [74]. In addition, the heterochromatin protein HPL-1, a chromodomain-containing reader, has been shown to recognize both H3K9 and H3K23 methylation [18]. Our data show that H3K23me3 is enriched at heterochromatin-associated regions and is linked to transcriptional repression. These observations suggest that H3K23me3 is an additional heterochromatin-associated repressive mark.

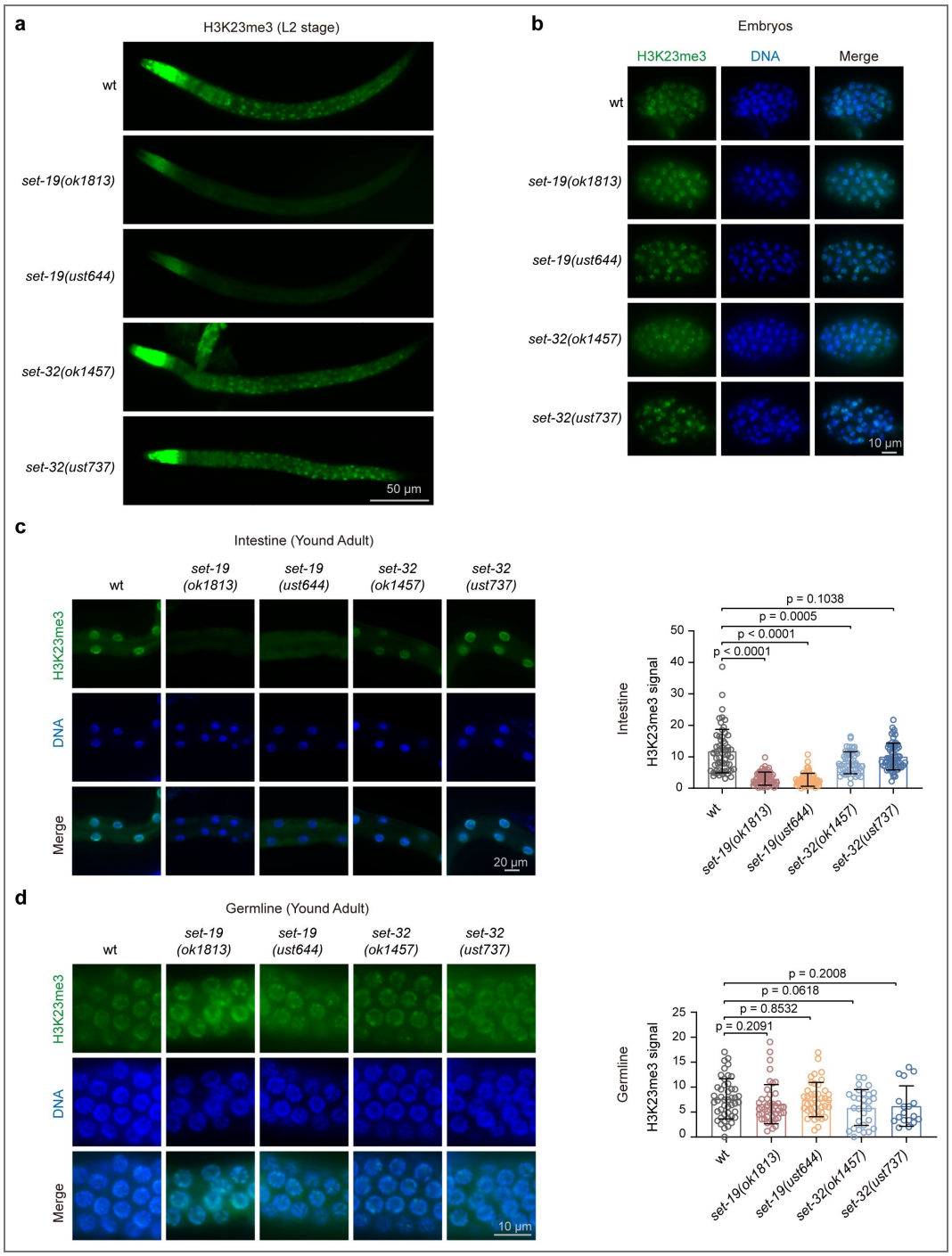

Fig. 6. SET-19 mediates H3K23me3 predominantly in somatic cells.

a, Representative immunofluorescence images of H3K23me3 staining in L2-stage worms. **b,** Representative H3K23me3 immunostaining in embryos. **c,** Representative images (left) and quantification of H3K23me3 immunostaining in the intestinal nuclei of young adult worms (right). H3K23me3 levels were calculated as nuclear fluorescence intensity after background subtraction, with three nuclei averaged per worm. H3K23me3 (green); DAPI (blue). Signal quantification was performed using ImageJ. A two-tailed t test was performed to determine statistical significance. For intestinal nuclei: wild type, *n* = 60 worms, *N* = 3 biological replicates; *set-19(ok1813)*, *n* = 60 worms, *N* = 3 biological replicates; *set-19(ust644)*, *n* = 60 worms, *N* = 3 biological replicates; *set-32(ok1457)*, *n* = 51 worms, *N* = 2 biological replicates; *set-32(ust737)*, *n* = 60 worms, *N* = 3 biological replicates. **d,** Representative images (left) and quantification of H3K23me3 immunostaining in the germline nuclei of young adult worms (right). H3K23me3 levels were calculated as nuclear fluorescence intensity after background subtraction, with three nuclei averaged per worm. H3K23me3 (green); DAPI (blue). Signal quantification was performed using ImageJ. A two-tailed t test was performed to determine statistical significance. For germline nuclei: wild type, *n* = 46 worms, *N* = 3 biological replicates; *set-19(ok1813)*, *n* = 44 worms, *N* = 3 biological replicates; *set-19(ust644)*, *n* = 42 worms, *N* = 2 biological replicates; *set-32(ok1457)*, *n* = 29 worms, *N* = 2 biological replicates; *set-32(ust737)*, *n* = 18 worms, *N* = 2 biological replicates.

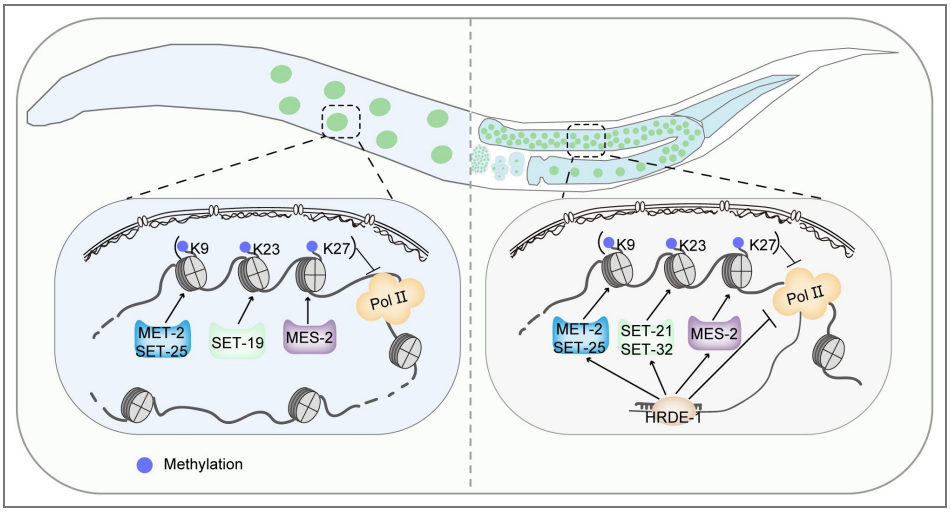

Fig. 7. A working model for somatic and germline H3K23 methylation in *C. elegans*.

(Left) In somatic cells, SET-19 acts as the major H3K23 methyltransferase. SET-19-catalyzed H3K23me3 coexists with H3K9me3 and H3K27me3 in heterochromatic regions and represses transcription. (Right) In the germ line, SET-32 and SET-21 participate in the maintenance of H3K23me3 downstream of the HRDE-1-mediated RNAi pathway and contribute to the transgenerational inheritance of RNAi.

Nevertheless, whether H3K23 methylation contributes to perinuclear chromatin organization remains an intriguing question. Future studies using perinuclear tethering assays could be used to assess the contribution of H3K23 methylation to nuclear positioning [74].

H3K23 methylation appears to be functionally distinct from other heterochromatin marks. The major H3K9 and H3K27 methyltransferases in *C. elegans*, MET-2/SET-25 and MES-2, respectively, act broadly across tissues and developmental stages [42,75]. In contrast, SET-19 contributes to H3K23me3 predominantly in somatic cells, pointing to distinct modes of enzymatic regulation among repressive histone modifications. This tissue-specific pattern of deposition further raises the possibility that different H3K23 methyltransferases may make distinct functional contributions. Although SET-32 has been linked to nuclear RNAi and transgenerational epigenetic inheritance in the germline [25,26,29,31,33,73], *set-19* mutants do not exhibit noticeable defects in feeding RNAi targeting either germline or somatic genes. These results indicate that SET-19 is not an indispensable requirement for the execution of feeding RNAi and its inheritance. However, whether SET-19 contributes to RNAi-induced H3K23me3 deposition in somatic cells requires further investigation.

While our findings support a predominantly somatic role for SET-19, the functions of H3K23 methylation in both somatic and germline cells remain to be fully defined. The unresolved questions include whether multiple H3K23 methyltransferases act redundantly or in parallel in the germline. It also remains unclear how SET-19-dependent and germline-enriched H3K23 methyltransferases are coordinated across tissues, and to what extent H3K23me3 overlaps functionally with other heterochromatin machineries. Systematic biochemical and genetic analyses of SET domain proteins in *C. elegans* will help define the full complement of histone methylation activities and clarify how chromatin-based regulation is directed to distinct developmental stages and cell types.

Materials and Methods

Strains

The Bristol strain N2 was used as the standard wild-type strain. All strains were grown at 20°C unless otherwise specified. The strains used in this study are listed in Table S1.

Construction of plasmids and transgenic strains

For in situ expression of GFP::SET-19, the coding sequence of 3×FLAG::GFP, fused to a linker sequence (GGAGGTGGAGGTGGAGCT), was inserted immediately downstream of the start codon of *set-19* using the CRISPR/Cas9 system. The 3×FLAG::GFP fragment was PCR-amplified from YY178 genomic DNA. Homologous left and right arms (1.5 kb each) were amplified from N2 genomic DNA, and the backbone fragment was amplified from plasmid pCFJ151. All fragments were assembled into the repair plasmid using the ClonExpress MultiS One Step Cloning Kit (C113-02, Vazyme) via Gibson assembly. The injection mixture contained pDD162 (50 ng/μl), the repair plasmid (50 ng/μl), pCFJ90 (5 ng/μl), and two or three sgRNA plasmids targeting sequences near the N-terminus of the *set-19* gene (20 ng/μl per sgRNA plasmid). The mixture was injected into adult animals. Three to four days after injection, F1 worms expressing pharyngeal GFP were isolated using a Leica M165 FC fluorescence stereomicroscope. Progeny from these F1 worms were subsequently screened by PCR and validated by Sanger sequencing. The sequences of primers used for construction of the in situ transgenic strain are listed in Table S2.

Construction of mutant strains via CRISPR/Cas9 technology

To generate sgRNA expression vectors, the 20 bp *unc-119* sgRNA guide sequence within the *pU6::unc-119* sgRNA(F+E) vector was replaced with distinct target-specific sgRNA guide sequences. A plasmid mixture containing 30 ng/μl of each of the three or four sgRNA expression vectors, 50 ng/μl of pDD162 plasmid, and 5 ng/μl of pSG259 was co-injected into wild-type N2 nematodes. Worms carrying the desired gene deletions were screened via PCR following the method described previously [76]. All sgRNA sequences used in this study are listed in Table S3.

Isolation of histones and mass spectrometry

Synchronized L3–L4 larvae and embryos (obtained by bleaching gravid adults) were washed three times with 1× M9 buffer. All samples were flash-frozen in liquid nitrogen and pulverized into a fine powder using a ball mill (60 Hz). The frozen powder was resuspended in Nuclear Extraction (NE) Buffer (100 mM HEPES, pH 7.5; 50 mM NaCl; 1% Triton X-100; 0.1% sodium deoxycholate; 1 mM EDTA; 10% glycerol; plus protease inhibitors). The resulting suspension was centrifuged at low speed to remove worm debris. To remove soluble proteins, the clarified supernatant was further centrifuged at high speed (16,000 × g for 10 min), and the resulting supernatant was discarded. The insoluble pellet was resuspended in NE buffer. Histone isolation was performed using a high-salt extraction strategy [77]. First, the insoluble pellet was further lysed in salt-free buffer to disrupt nuclear envelopes; histones were subsequently liberated from chromatin complexes via extraction with 2.5 M NaCl buffer. Histones were separated by SDS-PAGE, and the Coomassie blue-stained band containing histone H3 was cut from the gel. The gel slices underwent two rounds of propionylation with propionic anhydride to derivatize free and monomethylated lysine residues. Afterward, the samples were digested with trypsin, followed by an additional propionylation step to modify newly exposed N-terminal amines [39,78].

The eluted peptides were analyzed on an Easy-nLC 1000 system (Thermo Fisher) coupled to a Q Exactive mass spectrometer (Thermo Fisher) by LC-MS/MS. The acquired RAW data were analyzed using EpiProfile 2.1_Celegans, an updated version of EpiProfile 2.0 [79]. For each histone modified peptide, the relative abundance (%RA) was calculated by dividing the area under the curve (AUC) of each modified peptide by the sum of the areas corresponding to all the observed forms of that peptide.

Western blotting

Synchronized L3–L4 larvae and embryos obtained by bleaching gravid adults were washed three times with 1× M9 buffer. Samples were stored at -80°C until use. The samples were suspended in 2× SDS loading buffer and heated in a metal bath at 95°C for 5–10 minutes. The suspensions were then centrifuged at 16,000 × g, and the supernatants were collected. Proteins were resolved by SDS-PAGE on gradient gels (15% separation gel, 5% spacer gel) and transferred to a Hybond-ECL membrane. After washing with 1× Tris-buffered saline with Tween-20 (TBST) buffer and blocking with 5% milk-TBST, the membrane was incubated overnight at 4°C with antibodies. The membrane was washed three times for 10 minutes each with 1× TBST and then incubated with secondary antibodies at room temperature for 2 hours. The membrane was washed thrice for 10 minutes with 1× TBST and then visualized. The following antibodies were used for western blotting: anti-H3 (Abcam, ab1791), 1:8000; anti-H3K4me3 (Abcam, ab8580), 1:800; anti-H3K9me3 (Millipore, 07-523), 1:3000; anti-H3K27me3 (Millipore, 07-449), 1:8000; anti-H3K36me3 (Abcam, ab9050), 1:1000; anti-H3K23me1 (Active Motif, 39388), 1:6000; anti-H3K23me2 (Active Motif, 39653), 1:2000; anti-H3K23me2 (Beyotime, AG3990), 1:2000; anti-H3K23me3 (Active Motif, 61499), 1:3000; and anti-H3K23me3 (Beyotime, AG3889), 1:1000. Secondary antibodies: HRP-labeled goat anti-rabbit IgG (H+L) (Abcam, ab205718), 1:15000.

Recombinant protein expression and purification

The DNA segments encoding the SET domain of SET-19 (SET-19 SET; aa 37–318), the SET and coiled-coil domains of SET-19 (SET-19 SET+CC; aa 37–454) and the full-length protein of SET-32 were amplified from a cDNA library of wild-type strain N2 using PCR. Subsequently, the SET-19 SET, SET-19 SET+CC and SET-32 constructs were cloned and inserted into the pGEX-4T-1 plasmid and expressed in *E. coli* BL21-GOLD (DE3) cells (Novagen). The recombinant proteins were affinity-purified via GST tag binding to glutathione beads (Smart-Lifesciences, SA008100) according to the manufacturer's instructions. The eluted protein was dialyzed against a buffer containing 20 mM Tris-HCl pH 7.5, 5% glycerol, and 200 mM NaCl and subsequently concentrated. The concentrated protein was then subjected to high-speed centrifugation; after centrifugation, the clarified protein solution was supplemented with glycerol and stored at -80°C.

In vitro histone methylation assay

GST-fused proteins (0.25 μM) were incubated with 1 μM histone H3 (Active Motif, 31294) and 80 μM S-adenosylmethionine (SAM) (NEB, B9003S) in a 20 μl reaction mixture containing methyltransferase activity buffer (20 mM Tris-HCl, pH 8.0; 50 mM NaCl; 20 mM KCl; 10 mM $MgCl_2$; 5% glycerol; 0.02% Triton X-100; 0.1 mg/ml BSA; and 1 mM dithiothreitol [DTT]) for 3 h at 20°C. Reactions were terminated by the addition of SDS loading buffer, followed by boiling for 15 min. Proteins were resolved on a 15% SDS-PAGE gel and analyzed by western blotting.

Imaging

For imaging larval stages, animals were immobilized in 0.1 M sodium azide and mounted on 1.5% agarose pads. For imaging embryos and germ cells, gravid adults were dissected on a coverslip in 2 μl of 0.4× M9 buffer containing 0.1 M sodium azide and then mounted on freshly prepared 1.1% agarose pads. Imaging was performed using a Leica THUNDER Imaging System equipped with a K5 sCMOS camera and HC PL FLUOTAR objectives (100×/1.40–0.70 oil, 40×/0.80, and 20×/0.80). Images were acquired using Leica Application Suite X software (v3.7.4.23463).

Immunofluorescence staining and quantification

Embryos were freeze-cracked using liquid nitrogen, then fixed in methanol for 30 seconds and post-fixed in 1% paraformaldehyde (PFA) for 2 minutes. After three washes in PBS containing 0.25% Triton X-100 (PBS-T), samples were permeabilized in PBS with 1% Triton X-100 for 20 minutes. Subsequently, the samples were blocked in PBS containing 0.5% BSA before overnight incubation with the primary antibody against H3K23me3 (Active Motif, 61499) at 4°C. Following three washes with PBS-T, samples were incubated with secondary antibodies (Alexa Fluor 488-conjugated anti-rabbit) for 2 hours at room temperature, before three final PBS-T washes and DNA staining with Hoechst 33342. For germline and intestine staining, gravid adult worms were dissected in M9 buffer, fixed in methanol for 1 minute at -20°C and in 2% PFA for 5 minutes. For L2 worm staining, worms were freeze-cracked using liquid nitrogen, then fixed in 1% paraformaldehyde (PFA) for 20 minutes. Fixed animals were permeabilized by sequential thiol-based reduction and oxidation steps. Samples were incubated in PBS containing 10% β-mercaptoethanol for 15 minutes, treated with PBS containing 10 mM DTT for 15 minutes, and then incubated in PBS containing 0.3% H_2O_2 for 15 minutes. The animals were subsequently fixed in methanol for 30 seconds and treated with the permeabilization solution (PBS containing 1% Triton X-100) for 20 minutes. Images were taken on a Leica THUNDER Imaging System with identical gain settings within each experimental set. Quantification was performed using ImageJ by measuring the mean gray value within the nuclear region and that of an adjacent background area. For each worm or tissue, fluorescence intensity was calculated as the average nuclear signal from three nuclei, subtracting the average background signal from three corresponding adjacent background regions. At least two independent experiments were performed.

Brood Size

L4-stage hermaphrodites were singled onto plates and transferred daily as adults until embryo production ceased, and the progeny numbers were scored.

Hatch ratio

Synchronized adult hermaphrodites were transferred to NGM plates to lay eggs, which were subsequently removed. The numbers of embryos and hatched larvae were scored, and the hatch ratio was calculated as the number of hatched larvae divided by the total number of embryos.

Development rate

Synchronized adult hermaphrodites were transferred to NGM plates to lay eggs, which were subsequently removed. The growth of the progeny was monitored every 24 hours at 20°C.

RNAi

RNAi experiments were performed at 20°C by placing synchronized embryos on RNAi feeding plates as previously described [80]. HT115 bacteria expressing the empty vector L4440 (a gift from A. Fire) were used as controls. Bacterial clones expressing target-specific double-stranded RNAs (dsRNAs) were obtained from the Ahringer RNAi library [81] and their identities were verified by Sanger sequencing.

Total RNA isolation

Synchronized L4-stage worms were washed three times with 1× M9 to remove bacterial residues. For RNA extraction, 400 µl of TRIzol Reagent (Ambion, 15596026) was added to a 100 µl worm aliquot, followed by 7–8 cycles of freezing in liquid nitrogen and thawing in a 42°C water bath. Afterward, 100 µl of DNA/RNA Extraction Reagent (Solarbio LIFE SCIENCES, P1014) was added to the samples, which were then centrifuged at 16000 × g for 15 minutes at 4°C. The collected supernatant was further treated with 400 µl isopropanol and 400 µl pre-chilled 75% ethanol, and subjected to DNase I digestion (Thermo Fisher Scientific, EN0521). Finally, RNA was eluted into 20 µl of nuclease-free water and used for mRNA library preparation.

mRNA-seq analysis

The Illumina-generated raw reads were first filtered to remove adapters, low-quality reads, and contaminants, yielding high-quality clean reads. The clean reads were aligned to the reference genome of WBcel235 via HISAT2 (v2.1.0)[82]. For quantification, featureCounts (v1.6.0) [83] was used to calculate gene-level read counts. Library size factors were calculated using DESeq2 (v1.46.0) [84] with its standard median-of-ratios method based on genome-wide gene expression counts. Genes with an adjusted *P* value (padj) < 0.01 and an absolute log2FoldChange > 1 were considered significantly differentially expressed. Three biological replicates were analyzed per condition. All statistical analyses and plots were generated using custom R scripts.

Chromatin immunoprecipitation (ChIP)

ChIP experiments were performed as previously described [30]. For L3–L4 worms, frozen animals were first ground to a fine powder in liquid nitrogen [85]. Then, the samples were crosslinked in 2% formaldehyde for 10 minutes at room temperature with gentle rotation. Crosslinking was quenched by adding 0.125 M glycine (final concentration) for 5 minutes at room temperature. Samples were sonicated for 13 cycles (30 s on and 30 s off per cycle) at high output with a Bioruptor Plus (Diagenode), with the sample tubes kept in an ice-water bath throughout the process. The lysates were precleared and immunoprecipitated with a rabbit anti-H3K23me3 antibody (Active Motif, 61499) overnight at 4°C. Chromatin/antibody complexes were recovered with Dynabeads^{TM} Protein A (Invitrogen, 10002D) followed by extensive sequential washes with 150 mM, 500 mM, and 1 M NaCl, respectively. Crosslinks were reversed overnight at 65°C. The recovered DNA was treated with RNase (Roche) for 30 minutes at 65°C, and all DNA samples were purified using a DNA purification kit (TianGen, #DP204).

ChIP-Seq

The DNA samples from the ChIP experiments were subjected to quality control (QC) prior to sequencing and then sequenced at high depth at Novogene Bioinformatics Technology Co., Ltd. (Beijing, China). Briefly, the ChIP DNA was processed for library construction following the standard protocol: the DNA fragments were combined with an End Repair/A-tailing mix and incubated in a single reaction to complete end repair and 3'-end adenylation. The resulting A-tailed DNA fragments were then incubated with sequencing adapters in ligation mix to achieve adapter ligation. The adapter-ligated DNA was subjected to size selection and several rounds of PCR amplification to obtain the final DNA library. The size distribution of the library fragments was analyzed on the Agilent 5400 system (Agilent, USA; with matching Agilent assay reagents). The library was quantified by qPCR to a final concentration of 1.5 nM. The qualified libraries were

pooled according to their effective concentration and required data volume and then further amplified on cBot to generate clusters on the flow cell and sequenced with a paired-end 150 bp (PE150) method on an Illumina platform.

Published ChIP-seq datasets of histone modifications in *C. elegans* were downloaded from the NCBI GEO or ENCODE databases. The datasets used in this study are listed in Table S4.

ChIP-seq data analysis

ChIP-seq data analysis was performed as previously described [86]. ChIP-seq reads were aligned to the WBcel235 assembly of the *C. elegans* genome using Bowtie2 (v2.3.5.1) [87] by Ben Langmead with the default settings. The SAMtools (v0.1.19) [88] "view" utility was used to convert the alignments to BAM format, and the "sort" utility was used to sort the alignment files. ChIP-seq peaks were called using MACS2 (v2.1.1) [89] with subcommand. For the H3K4me3 and H3K36me3 datasets, which display narrow enrichment patterns, peaks were identified using the parameters "-g ce -B -f BAM -q 0.01". For the H3K27me3, H3K9me3, and H3K23me3 datasets, which show broad histone modification domains, peaks were identified using the parameters "-g ce -B -f BAMPE --broad --broad-cutoff 0.01". Deeptools subcommand bamCoverage (v3.5.0) was used to produce bigWig tracks for data visualization with defined parameters (--binSize 20 --normalizeUsing BPM --smoothLength 60 --extendReads 150) from bam files. The Integrative Genomics Viewer genome browser [90] was applied to visualize signals and peaks. The genomic regions were defined as chromosome arms and centers based on previous works [51]. For visualization of peak locations, we used the R package ggplot2 (v4.0.0).

For heatmap analysis, the called peaks of H3K23me3 rep1 were used. Deeptools subcommand computeMatrix (v3.4.3) was used to calculate the score matrix for the heatmap with defined parameters (reference-point --referencePoint center -b 3000 -a 3000 --skipZeros). The heatmap was plotted with Deeptools subcommand plotHeatmap (v3.5.0).

ChIPseqSpikeInFree normalization for H3K23me3

H3K23me3 ChIP-seq experiments were performed with two replicates each in both wild-type (wt) and *set-19* mutant backgrounds. To compare the H3K23me3 signals between the two backgrounds in the absence of spike-in, ChIPseqSpikeInFree (v1.2.4) [91] was used to calculate the scaling factor (SF) for every sample (SF_i). The effective ChIP-seq library size for sample i was calculated as $N_i * SF_i$, where N_i is the original library size. The effective library size was then used to normalize the read count from sample i during the downstream differential analysis and heatmap visualization. For the two replicates of wt and *set-19* mutants, pairwise comparisons were performed, and the resulting SF values were averaged, yielding SF_wt = 1 and SF_set-19 = 2.115. The "-scale" parameter for bedtools genomecov was calculated from the effective library size using the formula: Scale parameter = 15000000/(Ni × SFi), where 15000000 is the preset reference read count. Normalized BEDGraph files were generated by setting the "-scale" parameter to the value from the above formula. The genome was then partitioned into fixed 20 bp windows, and the normalized signal was mapped into these windows using a bedtools map with weighting by the actual overlap length. The $\log_2$(IP/Input) enrichment value for each window was subsequently calculated after adding a pseudocount of 1 to both IP and Input signals to avoid $\log_2(0)$ errors. Finally, the sorted BEDGraph file was converted into BigWig format for visualization. For the differential analysis of H3K23me3 peaks, we used the R package DiffBind (v3.16.0) [54] and integrated the sample-specific SF into the total read count normalization via the underlying DESeq2 (v1.46.0) [84] framework.

Statistics

Bar graphs with error bars are presented with mean and standard deviation (SD). All experiments were conducted with independent *C. elegans* animals for the indicated N times. Statistical analysis was performed with a two-tailed Student's t test.

Figure supplements

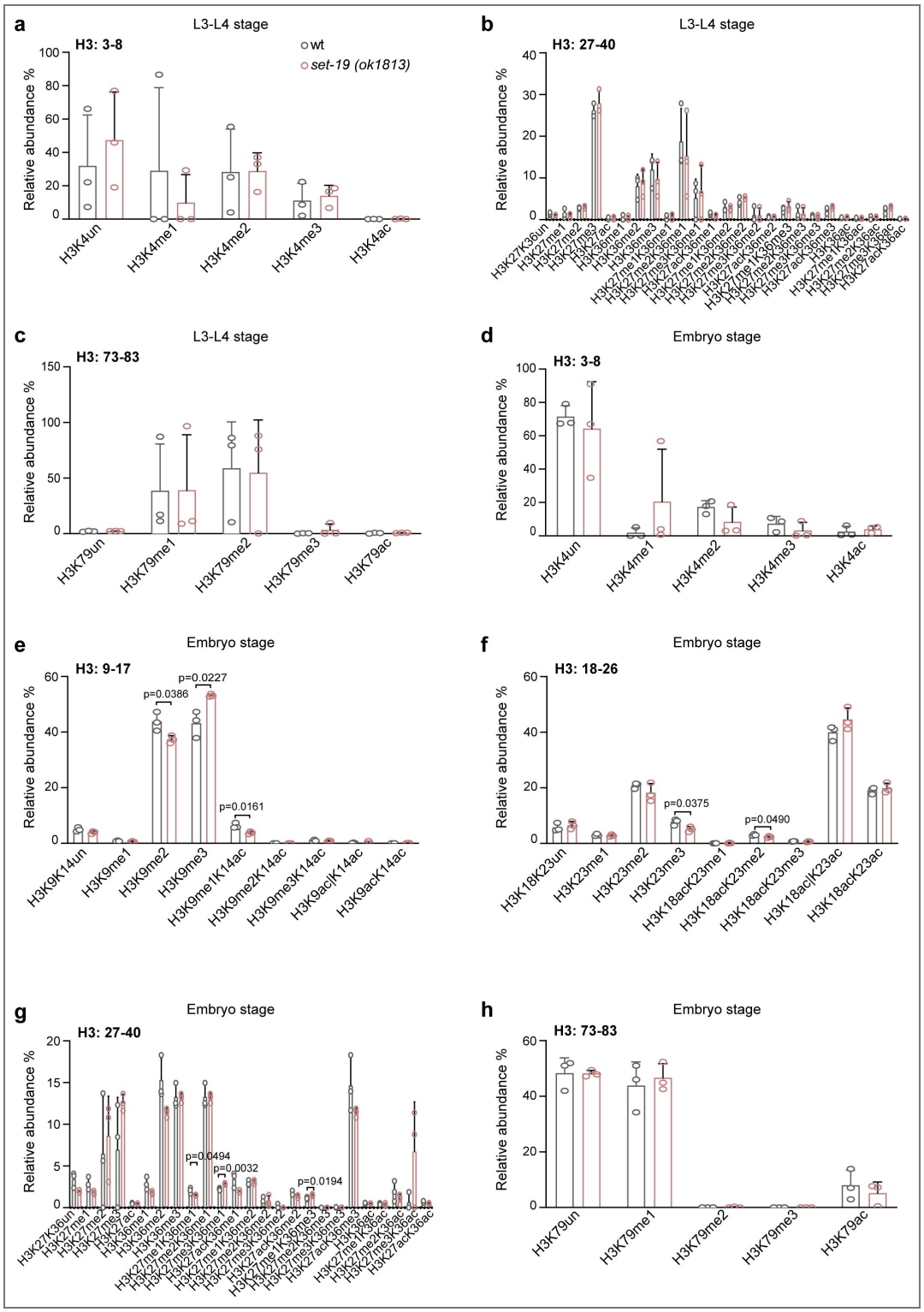

Fig. S1. Mass spectrometry analysis of global H3 methylation in *set-19(ok1813)* mutants. Quantification of H3 methylation levels in wild-type and *set-19(ok1813)* mutants by quantitative mass spectrometry. H3 methylation levels were quantified as relative abundances, calculated by dividing the area under the curve (AUC) of each modified peptide by the sum of the AUCs of all observed forms of that peptide and multiplying by 100. Differences without indicated p values are not statistically significant (two-tailed t test, $p < 0.05$). $N = 3$ biological replicates.

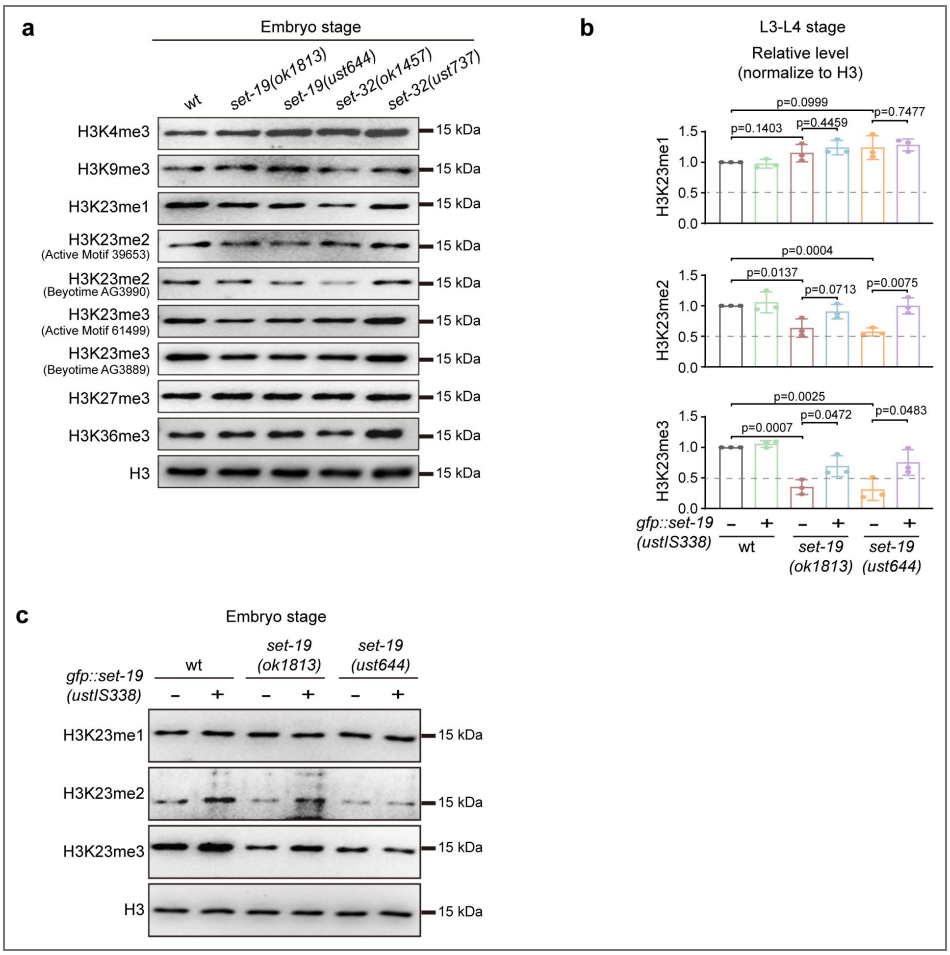

Fig. S2. The loss of *set-19* reduces H3K23 methylation levels.

a, Western blotting analysis of global H3 methylation levels in embryos of the indicated genotypes. **b,** Quantification of H3K23me1/2/3 levels in L3–L4 worms, related to Fig. 1f. *N* = 3 biological replicates; two-tailed t test. **c,** Western blotting analysis of H3K23me1/2/3 levels in embryos. The *fib-1p::gfp::set-19(ustIS338)* transgene was used for rescue.

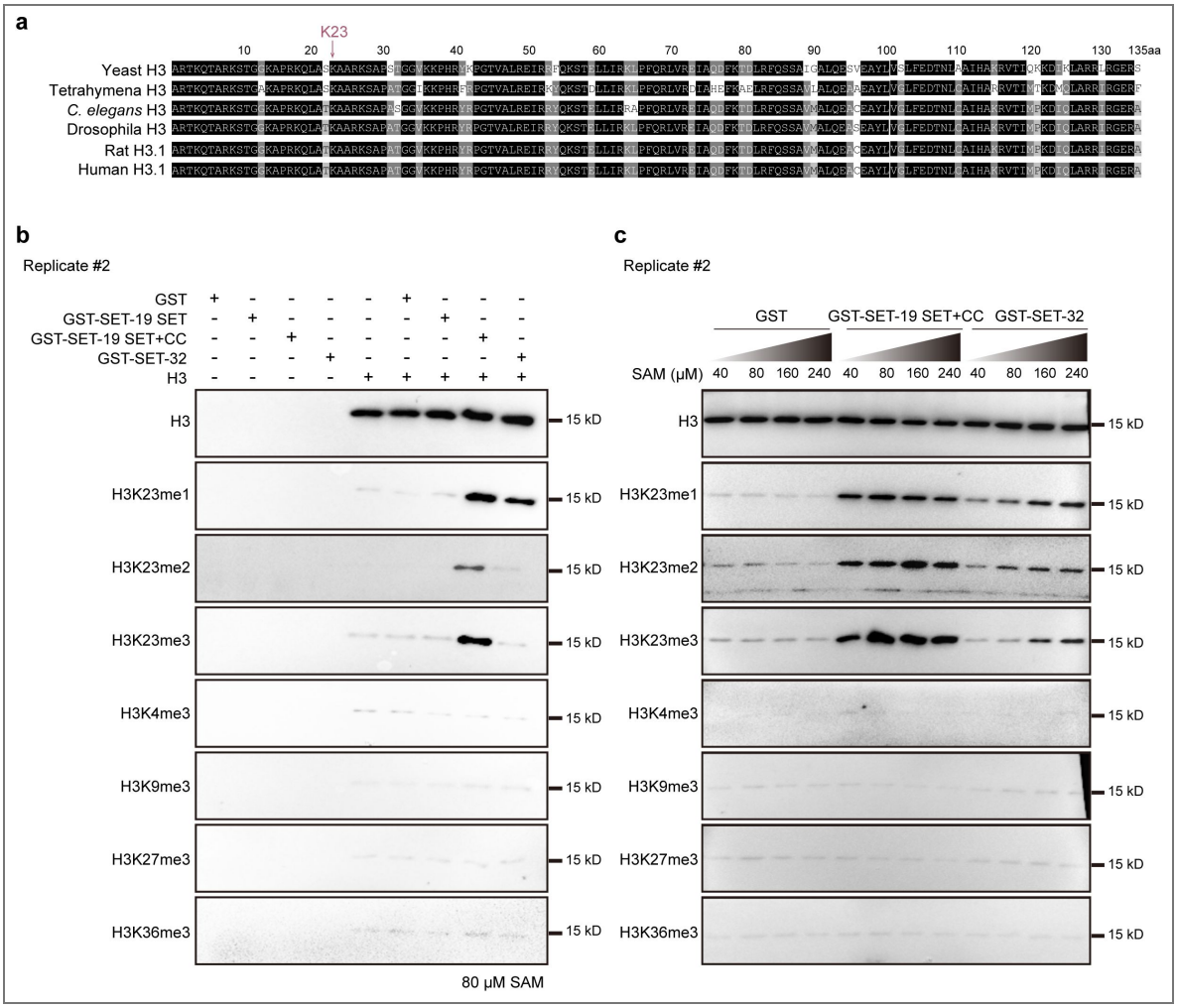

Fig. S3. SET-19 specifically catalyzes histone H3K23 methylation in vitro.

a, Multiple sequence alignment of histone H3 proteins across species, highlighting the conserved lysine 23 residue. **b, c,** Independent replicates of in vitro methylation assays corresponding to Fig. 2b and Fig. 2c, respectively.

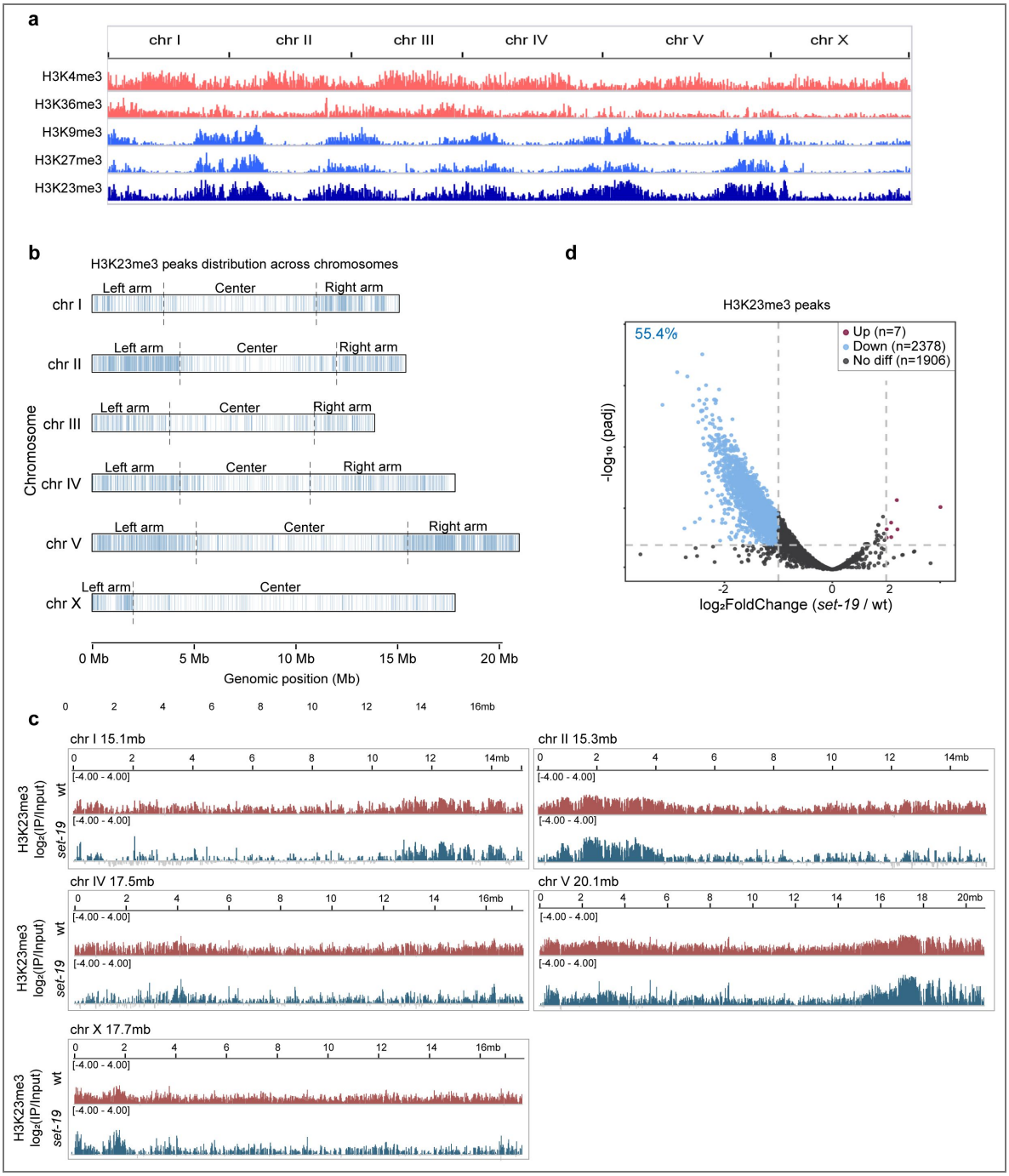

Fig. S4. The loss of *set-19* alters genomic H3K23me3 occupancy.

a, Genome-wide distribution of ChIP-seq peaks for H3K4me3, H3K36me3, H3K9me3, H3K27me3, and H3K23me3, as identified by MACS2. **b,** Distribution of H3K23me3 ChIP-seq peaks across chromosomes in wild-type worms. Peak positions identified by MACS2 from one representative biological replicate (replicate 1) are shown along each chromosome. Chromosome arms and centers are indicated. **c,** Comparison of H3K23me3 ChIP-seq signal distributions across chromosomes in wild-type and *set-19(ok1813)* worms. Mean $\log_2$ enrichment over input is shown (N = 2 biological replicates). **d,** Differential H3K23me3 peak analysis between *set-19(ok1813)* and wild-type worms. Volcano plot showing $\log_2$FoldChange (*set-19*/wt) versus -$\log_{10}$(adjusted p value [padj]) from DiffBind [54] analysis. Differentially enriched peaks are highlighted ($|\log_2\text{FoldChange}|>1$ and padj < 0.01). N = 2 biological replicates.

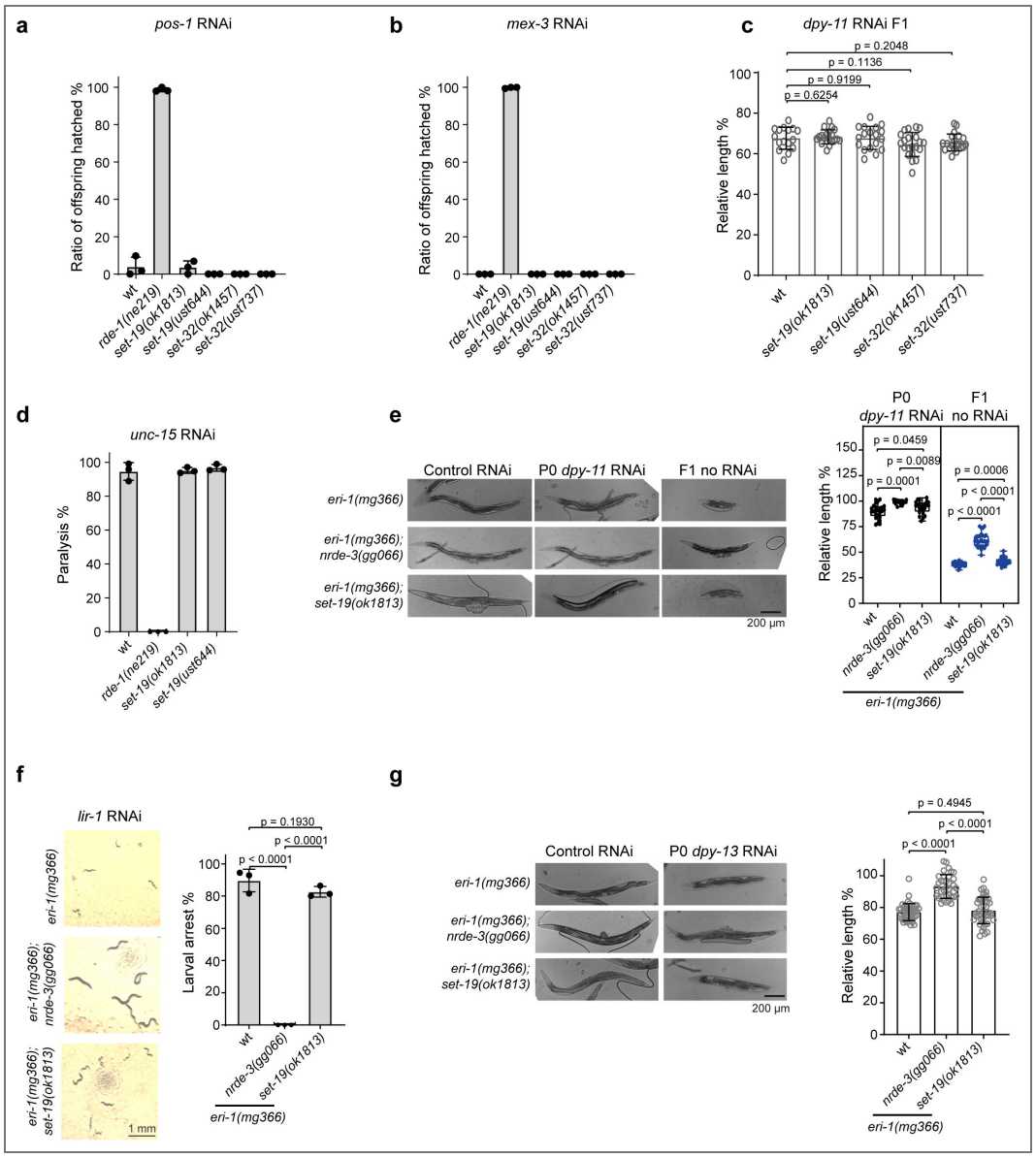

Fig. S5. SET-19 is dispensable for feeding RNAi responses.

a, b, Quantification of embryonic lethality following feeding RNAi targeting *pos-1* (**a**) or *mex-3* (**b**). Synchronized adult hermaphrodites of the indicated genotypes were exposed to dsRNA-expressing bacteria, and the ratio of hatched offspring was scored. **c,** Analysis of RNAi efficiency using *dpy-11* feeding RNAi. The indicated animals were exposed to *dpy-11* dsRNA until adulthood, and the relative body length of F1 progeny was measured. Individual data points represent single animals. **d,** Quantification of paralysis phenotypes following *unc-15* RNAi in the indicated genotypes. The percentage of paralyzed animals was scored. **e,** Animals of the indicated genotypes were exposed to *dpy-11* RNAi in the P0 generation and transferred to control bacteria. Representative images of P0 and F1 animals are shown (left). The relative body length of P0 and F1 animals was quantified (right). **f,** Larval arrest analysis following *lir-1* RNAi in the *eri-1(mg366)* background. Representative images of larvae are shown (left), and the percentage of animals exhibiting larval arrest was quantified (right). **g,** Analysis of the RNAi response to *dpy-13* feeding RNAi in the *eri-1(mg366)* background. The indicated animals were exposed to dsRNA until adulthood, and the relative body length was measured.

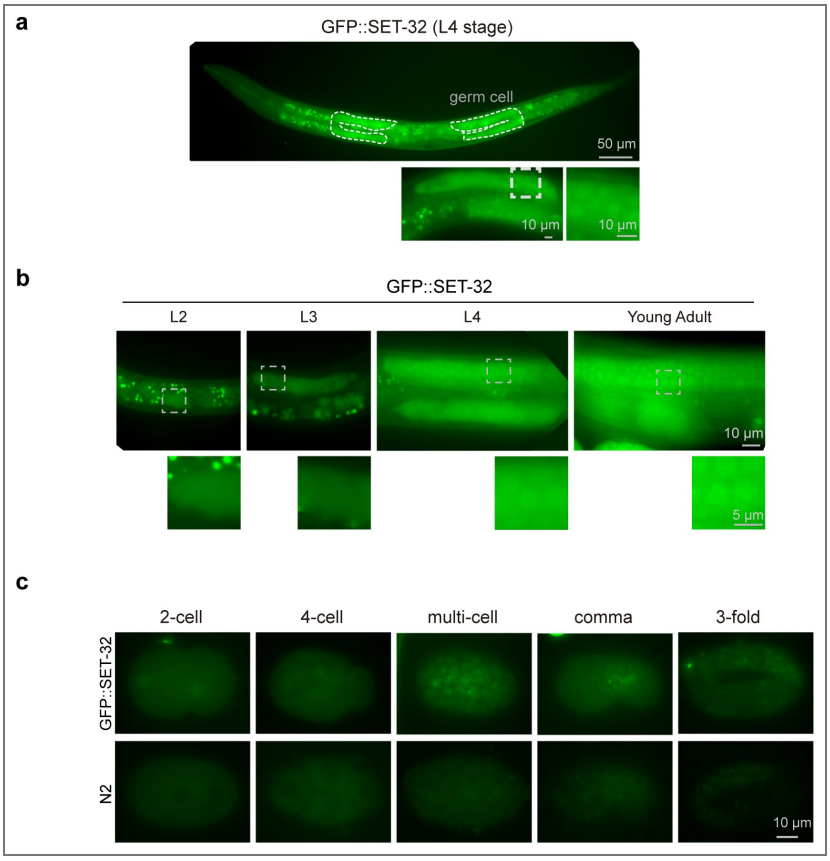

Fig. S6. Expression pattern of SET-32.

a, Fluorescence images of L4-stage animals expressing GFP::SET-32. **b,** Subcellular localization of GFP::SET-32 in the germline at different developmental stages. **c,** Subcellular localization of GFP::SET-32 in embryos.

Data availability

ChIP-seq and RNA-seq data have been deposited in the Genome Sequence Archive (GSA) at the National Genomics Data Center (NGDC) under accession number CRA037051. The mass spectrometry proteomics data have been deposited in the iProX repository with the accession codes IPX0015174000 and PXD073043. All data generated or analyzed during this study are included in the manuscript and supporting files. Source data files have been provided for all figures.

Acknowledgements

We are grateful to the members of the Guang laboratory for their comments and suggestions. We are grateful to the International *C. elegans* Gene Knockout Consortium and the National Bioresource Project for providing the strains. Some strains were provided by the CGC, which is funded by the NIH Office of Research Infrastructure Programs (P40 OD010440).

Additional information

Funding

This work was supported by grants from the National Key R&D Program of China (2022YFA1302700), the National Natural Science Foundation of China (32230016, 32270583, 32300438, 32400435, and 32470633), the Research Funds of Center for Advanced Interdisciplinary Science and Biomedicine of IHM (QYPY20230021), and the Fundamental Research Funds for the Central Universities (WK9100250107).

Author contributions

Y.S., M. Huang, X.F. and S.G. conceptualized the research; M.X., X.F. and S.G. designed the research; M.X., Z.F., M. Huang, and C.Y. performed the research; X.C., X. Huang, C.Z., M. Hong and X. Hou contributed new reagents; J.C., X. Hou, S.L. and M.L. provided technical guidance on bioinformatics analysis and protein purification; M.X., X.F. and S.G. wrote the paper.

Funding

Funder	Grant reference number	Author
MOST | National Key Research and Development Program of China (NKPs)	2022YFA1302700	Shouhong Guang
MOST | National Natural Science Foundation of China (NSFC)	32230016	Shouhong Guang
MOST | National Natural Science Foundation of China (NSFC)	32270583	Chengming Zhu
MOST | National Natural Science Foundation of China (NSFC)	32300438	Xinya Huang
MOST | National Natural Science Foundation of China (NSFC)	32400435	Xiangyang Chen
MOST | National Natural Science Foundation of China (NSFC)	32470633	Xuezhu Feng
MOE | Fundamental Research Funds for the Central Universities (Fundamental Research Fund for the Central Universities)	WK9100250107	Xiangyang Chen

Author ORCID iDs

Shouhong Guang: https://orcid.org/0000-0001-7700-9634

Additional files

Tables S1-S4.

References

1. **Millan-Zambrano G.,** Burton A., Bannister A. J., Schneider R (2022) Histone post-translational modifications - cause and consequence of genome function. *Nat. Rev. Genet* **23**:563-580 https://doi.org/10.1038/s41576-022-00468-7 | PubMed
2. **Nicetto D.,** et al. (2019) H3K9me3-heterochromatin loss at protein-coding genes enables developmental lineage specification. *Science* **363**:294-297 https://doi.org/10.1126/science.aau0583 | PubMed
3. **Methot S. P.,** et al. (2021) H3K9me selectively blocks transcription factor activity and ensures differentiated tissue integrity. *Nat. Cell Biol* **23**:1163-1175 https://doi.org/10.1038/s41556-021-00776-w | PubMed
4. **Zenk F.,** et al. (2017) Germ line–inherited H3K27me3 restricts enhancer function during maternal-to-zygotic transition. *Science* **357**:212-216 https://doi.org/10.1126/science.aam5339 | PubMed
5. **Völker-Albert M.,** Bronkhorst A., Holdenrieder S., Imhof A (2020) Histone modifications in stem cell development and their clinical implications. *Stem Cell Rep* **15**:1196-1205 https://doi.org/10.1016/j.stemcr.2020.11.002 | PubMed
6. **Campos E. I.,** Stafford J. M., Reinberg D (2014) Epigenetic inheritance: histone bookmarks across generations. *Trends Cell Biol* **24**:664-674 https://doi.org/10.1016/j.tcb.2014.08.004 | PubMed
7. **Wang Z. A.,** Cole P. A (2020) The chemical biology of reversible lysine post-translational modifications. *Cell Chem Biol* **27**:953-969 https://doi.org/10.1016/j.chembiol.2020.07.002 | PubMed
8. **Park J.,** Lee K., Kim K., Yi S. J (2022) The role of histone modifications: from neurodevelopment to neurodiseases. *Signal Transduct Target Ther* **7**:217 https://doi.org/10.1038/s41392-022-01078-9 | PubMed
9. **van Leeuwen F.,** Gafken P. R., Gottschling D. E (2002) Dot1p modulates silencing in yeast by methylation of the nucleosome core. *Cell* **109**:745-756 https://doi.org/10.1016/s0092-8674(02)00759-6 | PubMed
10. **Min J.,** Feng Q., Li Z., Zhang Y., Xu R.-M (2003) Structure of the catalytic domain of human DOT1L, a non-SET domain nucleosomal histone methyltransferase. *Cell* **112**:711-723 https://doi.org/10.1016/s0092-8674(03)00114-4 | PubMed
11. **Herz H.-M.,** Garruss A., Shilatifard A (2013) SET for life: biochemical activities and biological functions of SET domain-containing proteins. *Trends Biochem. Sci* **38**:621-639 https://doi.org/10.1016/j.tibs.2013.09.004 | PubMed
12. **Waterborg J. H** (1990) Sequence analysis of acetylation and methylation in two histone H3 variants of alfalfa. *J. Biol. Chem* **265**:17157-17161 https://doi.org/10.1016/s0021-9258(17)44882-4 | PubMed
13. **Garcia B. A.,** et al. (2007) Organismal differences in post-translational modifications in Histones H3 and H4. *J. Biol. Chem* **282**:7641-7655 https://doi.org/10.1074/jbc.m607900200 | PubMed
14. **Liu H.,** et al. (2010) Systematic identification of methyllysine-driven interactions for histone and nonhistone targets. *J. Proteome Res* **9**:5827-5836 https://doi.org/10.1021/pr100597b | PubMed
15. **Liu H.,** et al. (2013) A method for systematic mapping of protein lysine methylation identifies functions for HP1β in DNA damage response. *Mol. Cell* **50**:723-735 https://doi.org/10.1016/j.molcel.2013.04.025 | PubMed
16. **Zhang C. C.,** Molascon A. J., Gao S., Liu Y. F., Andrews P. C (2013) Quantitative proteomics reveals that the specific methyltransferases Txr1p and Ezl2p differentially affect the mono-, di- and trimethylation states of Histone H3 lysine 27 (H3K27). *Mol Cell Proteomics* **12**:1678-1688 https://doi.org/10.1074/mcp.m112.021733 | PubMed

17. **Papazyan R.,** et al. (2014) Methylation of histone H3K23 blocks DNA damage in pericentric heterochromatin during meiosis. *eLife* **3**:e02996 https://doi.org/10.7554/eLife.02996 | PubMed
18. **Vandamme J.,** et al. (2015) H3K23me2 is a new heterochromatic mark in *Caenorhabditis elegans*. *Nucleic Acids Res* **43**:9694-9710 https://doi.org/10.1093/nar/gkv1063 | PubMed
19. **Sidoli S.,** Vandamme J., Salcini A. E., Jensen O. N (2016) Dynamic changes of histone H3 marks during *Caenorhabditis elegans* lifecycle revealed by middle-down proteomics. *Proteomics* **16**:459-464 https://doi.org/10.1002/pmic.201500285 | PubMed
20. **Su Z.,** et al. (2016) Reader domain specificity and lysine demethylase-4 family function. *Nat. Commun* **7**:13387 https://doi.org/10.1038/ncomms13387 | PubMed
21. **Fišerová J.,** et al. (2017) Chromatin organization at the nuclear periphery as revealed by image analysis of structured illumination microscopy data. *J. Cell Sci* **130**:2066-2077 https://doi.org/10.1242/jcs.198424 | PubMed
22. **Myers T. R.,** et al. (2018) JMJD-1.2 controls multiple histone post-translational modifications in germ cells and protects the genome from replication stress. *Sci. Rep* **8**:3765 https://doi.org/10.1038/s41598-018-21914-9 | PubMed
23. **Lin T.,** et al. (2020) Changes of histone H3 lysine 23 acetylation and methylation in porcine somatic cells, oocytes and preimplantation embryos. *Theriogenology* **148**:162-173 https://doi.org/10.1016/j.theriogenology.2020.03.006 | PubMed
24. **Trejo-Arellano M.,** et al. (2017) H3K23me1 is an evolutionarily conserved histone modification associated with CG DNA methylation in Arabidopsis. *Plant J* **90**:293-303 https://doi.org/10.1111/tpj.13489 | PubMed
25. **Schwartz-Orbach L.,** et al. (2020) *Caenorhabditis elegans* nuclear RNAi factor SET-32 deposits the transgenerational histone modification, H3K23me3. *eLife* **9**:e54309 https://doi.org/10.7554/eLife.54309 | PubMed
26. **Zhebrun A.,** et al. (2025) Two H3K23 histone methyltransferases, SET-32 and SET-21, function synergistically to promote nuclear RNAi-mediated transgenerational epigenetic inheritance in *Caenorhabditis elegans*. *Genetics* **229**:iyae206 https://doi.org/10.1093/genetics/iyae206 | PubMed
27. **Gu S. G.,** et al. (2012) Amplification of siRNA in *Caenorhabditis elegans* generates a transgenerational sequence-targeted histone H3 lysine 9 methylation footprint. *Nat. Genet* **44**:157-164 https://doi.org/10.1038/ng.1039 | PubMed
28. **Buckley B. A.,** et al. (2012) A nuclear Argonaute promotes multigenerational epigenetic inheritance and germline immortality. *Nature* **489**:447-451 https://doi.org/10.1038/nature11352 | PubMed
29. **Kalinava N.,** Ni J. Z., Peterman K., Chen E., Gu S. G (2017) Decoupling the downstream effects of germline nuclear RNAi reveals that H3K9me3 is dispensable for heritable RNAi and the maintenance of endogenous siRNA-mediated transcriptional silencing in *Caenorhabditis elegans*. *Epigenetics Chromatin* **10**:6 https://doi.org/10.1186/s13072-017-0114-8 | PubMed
30. **Mao H.,** et al. (2015) The Nrde pathway mediates small-RNA-directed histone H3 lysine 27 trimethylation in *Caenorhabditis elegans*. *Curr. Biol* **25**:2398-2403 https://doi.org/10.1016/j.cub.2015.07.051 | PubMed
31. **Woodhouse R. M.,** et al. (2018) Chromatin modifiers SET-25 and SET-32 are required for establishment but not long-term maintenance of transgenerational epigenetic inheritance. *Cell Rep* **25**:2259-2272.e2255 https://doi.org/10.1016/j.celrep.2018.10.085 | PubMed
32. **Kalinava N.,** et al. (2018) *C. elegans* heterochromatin factor SET-32 plays an essential role in transgenerational establishment of nuclear RNAi-mediated epigenetic silencing. *Cell Rep* **25**:2273-2284.e2273 https://doi.org/10.1016/j.celrep.2018.10.086 | PubMed
33. **Spracklin G.,** et al. (2017) The RNAi Inheritance Machinery of *Caenorhabditis elegans*. *Genetics* **206**:1403-1416 https://doi.org/10.1534/genetics.116.198812 | PubMed

34. **Ahringer J.,** Gasser S. M (2018) Repressive chromatin in *Caenorhabditis elegans*: establishment, composition, and function. *Genetics* **208**:491-511 https://doi.org/10.1534/genetics.117.300386 | PubMed

35. **Li T.,** Kelly W. G (2011) A role for Set1/MLL-related components in epigenetic regulation of the *Caenorhabditis elegans* germ line. *PLoS Genet* **7**:e1001349 https://doi.org/10.1371/journal.pgen.1001349 | PubMed

36. **Robert Valérie J.,** et al. (2014) The SET-2/SET1 histone H3K4 methyltransferase maintains pluripotency in the *Caenorhabditis elegans* germline. *Cell Rep* **9**:443-450 https://doi.org/10.1016/j.celrep.2014.09.018 | PubMed

37. **Xiao Y.,** et al. (2011) *Caenorhabditis elegans* chromatin-associated proteins SET-2 and ASH-2 are differentially required for histone H3 Lys 4 methylation in embryos and adult germ cells. *Proc. Natl. Acad. Sci. U.S.A* **108**:8305-8310 https://doi.org/10.1073/pnas.1019290108 | PubMed

38. **Ni Z.,** Ebata A., Alipanahiramandi E., Lee S. S (2012) Two SET domain containing genes link epigenetic changes and aging in *Caenorhabditis elegans*. *Aging Cell* **11**:315-325 https://doi.org/10.1111/j.1474-9726.2011.00785.x | PubMed

39. **Towbin B. D.,** et al. (2012) Step-wise methylation of histone H3K9 positions heterochromatin at the nuclear periphery. *Cell* **150**:934-947 https://doi.org/10.1016/j.cell.2012.06.051 | PubMed

40. **Padeken J.,** et al. (2021) Argonaute NRDE-3 and MBT domain protein LIN-61 redundantly recruit an H3K9me3 HMT to prevent embryonic lethality and transposon expression. *Genes Dev* **35**:82-101 https://doi.org/10.1101/gad.344234.120 | PubMed

41. **Bessler J. B.,** Andersen E. C., Villeneuve A. M (2010) Differential localization and independent acquisition of the H3K9me2 and H3K9me3 chromatin modifications in the *Caenorhabditis elegans* adult germ line. *PLoS Genet* **6**:e1000830 https://doi.org/10.1371/journal.pgen.1000830 | PubMed

42. **Bender L. B.,** Cao R., Zhang Y., Strome S (2004) The MES-2/MES-3/MES-6 complex and regulation of histone H3 methylation in *C. elegans*. *Curr. Biol* **14**:1639-1643 https://doi.org/10.1016/j.cub.2004.08.062 | PubMed

43. **Furuhashi H.,** et al. (2010) Trans-generational epigenetic regulation of *C. elegans* primordial germ cells. *Epigenetics Chromatin* **3**:15 https://doi.org/10.1186/1756-8935-3-15 | PubMed

44. **Greer E. L.,** et al. (2014) A histone methylation network regulates transgenerational epigenetic memory in *C. elegans*. *Cell Rep* **7**:113-126 https://doi.org/10.1016/j.celrep.2014.02.044 | PubMed

45. **Zeng C.,** et al. (2026) A SET domain-containing protein and HCF-1 maintain transgenerational epigenetic memory. *Nat. Commun* **17**:1462 https://doi.org/10.1038/s41467-025-68200-7 | PubMed

46. **Huang M.,** et al. (2022) H3K9me1/2 methylation limits the lifespan of *daf-2* mutants in *C. elegans*. *eLife* **11**:e74812 https://doi.org/10.7554/eLife.74812 | PubMed

47. **Dai Z.,** Ramesh V., Locasale J. W (2020) The evolving metabolic landscape of chromatin biology and epigenetics. *Nat. Rev. Genet* **21**:737-753 https://doi.org/10.1038/s41576-020-0270-8 | PubMed

48. **Serefidou M.,** Venkatasubramani A. V., Imhof A (2019) The impact of one carbon metabolism on histone methylation. *Front. Genet* **10**:764 https://doi.org/10.3389/fgene.2019.00764 | PubMed

49. **Mentch S. J.,** et al. (2015) Histone methylation dynamics and gene regulation occur through the sensing of one-carbon metabolism. *Cell Metab* **22**:861-873 https://doi.org/10.1016/j.cmet.2015.08.024 | PubMed

50. **Haws S. A.,** et al. (2023) Intrinsic catalytic properties of histone H3 lysine-9 methyltransferases preserve monomethylation levels under low S-adenosylmethionine. *J. Biol. Chem* **299**:104938 https://doi.org/10.1016/j.jbc.2023.104938 | PubMed

51. **Liu T.,** et al. (2011) Broad chromosomal domains of histone modification patterns in *C. elegans*. *Genome Res* **21**:227-236 https://doi.org/10.1101/gr.115519.110 | PubMed

52. **Rockman M. V.,** Kruglyak L (2009) Recombinational landscape and population genomics of *Caenorhabditis elegans*. *PLoS Genet* **5**:e1000419 https://doi.org/10.1371/journal.pgen.1000419 | PubMed

53. **Barnes T. M.,** Kohara Y., Coulson A., Hekimi S (1995) Meiotic recombination, noncoding DNA and genomic organization in *Caenorhabditis elegans*. *Genetics* **141**:159-179 https://doi.org/10.1093/genetics/141.1.159 | PubMed

54. **Ross-Innes C. S.,** et al. (2012) Differential oestrogen receptor binding is associated with clinical outcome in breast cancer. *Nature* **481**:389-393 https://doi.org/10.1038/nature10730 | PubMed

55. **Lev I.,** Gingold H., Rechavi O (2019) H3K9me3 is required for inheritance of small RNAs that target a unique subset of newly evolved genes. *eLife* **8**:e40448 https://doi.org/10.7554/eLife.40448 | PubMed

56. **Tabara H.,** Hill R., Mello C., Priess J., Kohara Y. (1999) *pos-1* encodes a cytoplasmic zinc-finger protein essential for germline specification in *C. elegans*. *Development* **126**:1-11 https://doi.org/10.1242/dev.126.1.1 | PubMed

57. **Draper B.,** Mello C., Bowerman B., Hardin J., Priess J (1996) MEX-3 is a KH domain protein that regulates blastomere identity in early *C. elegans* embryos. *Cell* **87**:205-216 https://doi.org/10.1016/s0092-8674(00)81339-2 | PubMed

58. **Tabara H.,** et al. (1999) The *rde-1* gene, RNA interference, and transposon silencing in C. elegans. *Cell* **99**:123-132 https://doi.org/10.1016/s0092-8674(00)81644-x | PubMed

59. **Ko F.,** Chow K (2002) A novel thioredoxin-like protein encoded by the *C. elegans dpy-11* gene is required for body and sensory organ morphogenesis. *Development* **129**:1185-1194 https://doi.org/10.1242/dev.129.5.1185 | PubMed

60. **Guang S.,** et al. (2008) An Argonaute transports siRNAs from the cytoplasm to the nucleus. *Science* **321**:537-541 https://doi.org/10.1126/science.1157647 | PubMed

61. **Rose A.,** Baillie D (1980) Genetic organization of the region around UNC-15 (I), a gene affecting paramyosin in *Caenorhabditis elegans*. *Genetics* **96**:639-648 https://doi.org/10.1093/genetics/96.3.639 | PubMed

62. **Steiner F.,** Okihara K., Hoogstrate S., Sijen T., Ketting R (2009) RDE-1 slicer activity is required only for passenger-strand cleavage during RNAi in *Caenorhabditis elegans*. *Nat. Struct. Mol. Biol* **16**:207-211 https://doi.org/10.1038/nsmb.1541 | PubMed

63. **von Mende N.,** Bird D., Albert P., Riddle D. (1988) *dpy-13*: a nematode collagen gene that affects body shape. *Cell* **55**:567-576 https://doi.org/10.1016/0092-8674(88)90215-2 | PubMed

64. **Bosher J.,** Dufourcq P., Sookhareea S., Labouesse M (1999) RNA interference can target pre-mRNA: consequences for gene expression in a *Caenorhabditis elegans* operon. *Genetics* **153**:1245-1256 https://doi.org/10.1093/genetics/153.3.1245 | PubMed

65. **Cao J.,** et al. (2017) Comprehensive single-cell transcriptional profiling of a multicellular organism. *Science* **357**:661-667 https://doi.org/10.1126/science.aam8940 | PubMed

66. **Fisher K.,** Southall S. M., Wilson J. R., Poulin G. B (2010) Methylation and demethylation activities of a *C. elegans* MLL-like complex attenuate RAS signalling. *Developmental Biology* **341**:142-153 https://doi.org/10.1016/j.ydbio.2010.02.023 | PubMed

67. **Yuan J.,** et al. (2020) Two conserved epigenetic regulators prevent healthy ageing. *Nature* **579**:118-122 https://doi.org/10.1038/s41586-020-2037-y | PubMed

68. **Su L.,** et al. (2018) Muscle-specific histone H3K36 dimethyltransferase SET-18 shortens lifespan of *Caenorhabditis elegans* by repressing daf-16a expression. *Cell Rep* **22**:2716-2729 https://doi.org/10.1016/j.celrep.2018.02.029 | PubMed

69. **Rechtsteiner A.,** et al. (2010) The histone H3K36 methyltransferase MES-4 acts epigenetically to transmit the memory of germline gene expression to progeny. *PLoS Genetics* **6**:e1001091 https://doi.org/10.1371/journal.pgen.1001091 | PubMed

70. **Irvine D. V.,** et al. (2006) Argonaute slicing is Required for heterochromatic silencing and spreading. *Science* **313**:1134-1137 https://doi.org/10.1126/science.1128813 | PubMed

71. **Volpe T. A.,** et al. (2002) Regulation of heterochromatic silencing and histone H3 lysine-9 methylation by RNAi. *Science* **297**:1833-1837 https://doi.org/10.1126/science.1074973 | PubMed

72. **Burton N. O.,** et al. (2011) Nuclear RNAi maintains heritable gene silencing in *Caenorhabditis elegans*. *Proc. Natl. Acad. Sci. U.S.A* **108**:19683-19688 https://doi.org/10.1073/pnas.1113310108 | PubMed

73. **Ashe A.,** et al. (2012) piRNAs can trigger a multigenerational epigenetic memory in the germline of *C. elegans*. *Cell* **150**:88-99 https://doi.org/10.1016/j.cell.2012.06.018 | PubMed

74. **Meister P.,** et al. (2010) The spatial dynamics of tissue-specific promoters during *C. elegans* development. *Genes Dev* **24**:766-782 https://doi.org/10.1101/gad.559610 | PubMed

75. **Zeller P.,** et al. (2016) Histone H3K9 methylation is dispensable for *Caenorhabditis elegans* development but suppresses RNA:DNA hybrid-associated repeat instability. *Nat. Genet* **48**:1385-1395 https://doi.org/10.1038/ng.3672 | PubMed

76. **Chen X.,** et al. (2014) Dual sgRNA-directed gene knockout using CRISPR/Cas9 technology in *Caenorhabditis elegans*. *Sci. Rep* **4**:7581 https://doi.org/10.1038/srep07581 | PubMed

77. **Shechter D.,** Dormann H. L., Allis C. D., Hake S. B (2007) Extraction, purification and analysis of histones. *Nat. Protoc* **2**:1445-1457 https://doi.org/10.1038/nprot.2007.202 | PubMed

78. **Garcia B. A.,** et al. (2007) Chemical derivatization of histones for facilitated analysis by mass spectrometry. *Nat. Protoc* **2**:933-938 https://doi.org/10.1038/nprot.2007.106 | PubMed

79. **Yuan Z.-F.,** et al. (2018) EpiProfile 2.0: A computational platform for processing epi-proteomics mass spectrometry data. *J. Proteome Res* **17**:2533-2541 https://doi.org/10.1021/acs.jproteome.8b00133 | PubMed

80. **Timmons L.,** Court D. L., Fire A (2001) Ingestion of bacterially expressed dsRNAs can produce specific and potent genetic interference in *Caenorhabditis elegans*. *Gene* **263**:103-112 https://doi.org/10.1016/s0378-1119(00)00579-5 | PubMed

81. **Kamath R. S.,** et al. (2003) Systematic functional analysis of the *Caenorhabditis elegans* genome using RNAi. *Nature* **421**:231-237 https://doi.org/10.1038/nature01278 | PubMed

82. **Kim D.,** et al. (2019) Graph-based genome alignment and genotyping with HISAT2 and HISAT-genotype. *Nat. Biotechnol* **37**:907-915 https://doi.org/10.1038/s41587-019-0201-4 | PubMed

83. **Liao Y.,** Smyth G. K., Shi W (2014) featureCounts: an efficient general purpose program for assigning sequence reads to genomic features. *Bioinformatics* **30**:923-930 https://doi.org/10.1093/bioinformatics/btt656 | PubMed

84. **Love M. I.,** Huber W., Anders S (2014) Moderated estimation of fold change and dispersion for RNA-seq data with DESeq2. *Genome Biol* **15**:550 https://doi.org/10.1186/s13059-014-0550-8 | PubMed

85. **Kolasinska-Zwierz P.,** et al. (2009) Differential chromatin marking of introns and expressed exons by H3K36me3. *Nat. Genet* **41**:376-381 https://doi.org/10.1038/ng.322 | PubMed

86. **Hou X.,** et al. (2023) Systematic characterization of chromodomain proteins reveals an H3K9me1/2 reader regulating aging in *C. elegans*. *Nat. Commun* **14**:1254 https://doi.org/10.1038/s41467-023-36898-y | PubMed

87. **Langmead B.,** Salzberg S. L (2012) Fast gapped-read alignment with Bowtie 2. *Nat. Methods* **9**:357-359 https://doi.org/10.1038/nmeth.1923 | PubMed

88. **Li H.,** et al. (2009) The Sequence Alignment/Map format and SAMtools. *Bioinformatics* **25**:2078-2079 https://doi.org/10.1093/bioinformatics/btp352 | PubMed

89. **Zhang Y.,** et al. (2008) Model-based analysis of ChIP-Seq (MACS). *Genome Biology* **9**:R137 https://doi.org/10.1186/gb-2008-9-9-r137 | PubMed

90. **Robinson J. T.,** et al. (2011) Integrative Genomics Viewer. *Nat. Biotechnol.* **29**:24-26 https://doi.org/10.1038/nbt.1754 | PubMed

91. **Jin H.,** et al. (2019) ChIPseqSpikeInFree: a ChIP-seq normalization approach to reveal global changes in histone modifications without spike-in. *Bioinformatics* **36**:1270-1272 https://doi.org/10.1093/bioinformatics/btz720 | PubMed

Xu M., et al. (2026) Identification of a somatic H3K23me3 methyltransferase SET-19 in C. elegans. Genome Sequence Archive. ID CRA037051 https://ngdc.cncb.ac.cn/gsa/browse/CRA037051

Xu M., et al. (2026) Identification of a somatic H3K23me3 methyltransferase SET-19 in C. elegans. iProX. ID IPX0015174000 https://www.iprox.cn/page/project.html?id=IPX0015174000

Xu M., et al. (2026) Identification of a somatic H3K23me3 methyltransferase SET-19 in C. elegans. iProX. ID IPX0015174000 https://www.iprox.cn/page/project.html?id=IPX0015174000

Jänes J., et al. (2018) Chromatin accessibility dynamics across C. elegans development and ageing. NCBI Sequence Read Archive. ID SRR7164162 https://www.ncbi.nlm.nih.gov/sra/?term=SRR7164162

McMurchy A. N., et al. (2017) A team of heterochromatin factors collaborates with small RNA pathways to combat repetitive elements and germline stress. NCBI Sequence Read Archive. ID SRR5297105 https://www.ncbi.nlm.nih.gov/sra/?term=SRR5297105

Jänes J., et al. (2018) Chromatin accessibility dynamics across C. elegans development and ageing. NCBI Sequence Read Archive. ID SRR7164198 https://www.ncbi.nlm.nih.gov/sra/?term=SRR7164198

Jänes J., et al. (2018) Chromatin accessibility dynamics across C. elegans development and ageing. NCBI Sequence Read Archive. ID SRR7164186 https://www.ncbi.nlm.nih.gov/sra/?term=SRR7164186

Peer reviews

Reviewer #1 (Public review):

Summary:

The authors wanted to determine whether the set-19 gene, one of 38 SET-domain containing genes in C elegans, has a clear function in vivo with respect to lysine methylation. The question is not only whether it can modify this histone tail residue, but also what the impact of a loss of this locus is on the inheritance of repressive chromatin states.

Strengths:

The authors clearly achieved their goal, and it is convincingly shown that SET_19 is indeed a somatic cell histone methyltransferase with a striking specificity for H3K23. There is both recombinant protein work, quantitative mapping in vivo, of histone marks and transcriptional changes, and the authors rule out some other hypotheses that have been in the literature. Overall, this provides a compelling argument that SET-19 is indeed the major somatic cell HMT for this residue. Interestingly, the phenotypes are rather minimal, consistent with redundancy in the physiological roles of histone methylation, and redundancy as well in HMT function. For the most part, the data are not over-interpreted. The genetic alleles used, assuming they are confirmed, were revealing and well-documented.

Weaknesses:

The major weaknesses are easily fixed. The major weaknesses mainly reflect a slight overstatement of certain data (claiming insignificance, when it is not clear how that was determined) and claiming a bit too much about SET-32, which was independently claimed to be an H3K23 HMT. Clearly, the two SET domain enzymes are not redundant, nor is the claim that SET-32 has no role in H3K23 methylation completely convincing. Especially in germline or embryonic conditions. Finally, the imaging is not of very high quality, nor are the images fully quantitated. These points can be easily remedied.

https://doi.org/10.7554/eLife.111326.1.sa2

Reviewer #2 (Public review):

Summary:

This manuscript identifies SET-19 as a somatic H3K23 methyltransferase in C. elegans,

building on previous genetic evidence for a role of set-19 in H3K23me3 regulation. The authors combine quantitative mass spectrometry, western blotting, in vitro methyltransferase assays, ChIP-seq, and RNA-seq to show that loss of set-19 causes a strong reduction of H3K23me3, particularly in somatic tissues, and is associated with derepression of a subset of genes enriched for H3K23me3. They further conclude that SET-19 is dispensable for canonical feeding RNAi and for transgenerational or intergenerational inheritance of RNAi, distinguishing its function from other heterochromatin-associated methyltransferases such as SET-25, SET-32, and the H3K27 HMTs. Overall, the work adds an important piece to the H3K23 methylation pathway and tissue-specific chromatin regulation in C. elegans.

Strengths:

Very strong genetic and biochemical evidence for SET-19 as the major H3K23me3 HMT.

The mass spectrometry and western blot data convincingly demonstrate a strong reduction of H3K23me3 in two independent set-19 alleles and rescue by GFP::SET-19, which is a major strength (Figure 1, including Figure 1f).

The in vitro methyltransferase assays (Figure 2) showing robust H3K23me1/2/3 activity for SET-19 SET+CC and only modest H3K23me activity for SET-32, together with the SAM titration experiment in Figure 2C, are very informative and nicely support the conclusion that SET-19 is a high-activity H3K23 methyltransferase compared to SET-32.

The ChIP-seq analysis is central to the conclusions that H3K23me3 is enriched on chromosome arms, co-localizes with H3K9me3/H3K27me3, and is strongly reduced in set-19 mutants.

Weaknesses:

(1) The global reduction of H3K23me3 in Figure 3b,c and Figure S4c is convincing, but the correlation analysis between H3K23me3 loss and mRNA changes in Figure 3g could be strengthened. Currently, the analysis appears to focus on broad categories; it would be helpful to provide:

Representative genome browser tracks (e.g., exemplary gene coverage plots) for several genes that show clear H3K23me3 peaks in wild type, reduction in set-19, and concomitant upregulation of mRNA levels, and for a few genes that retain H3K23me3 and do not change expression. This would make the link between chromatin changes and transcriptional output more concrete.

(2) In Figure S4C, the authors note a pronounced reduction of H3K23me3 mainly on chromosome arms, but in the current data, it appears that the impact might be arm-specific (i.e., stronger reduction in one arm than the other in a chromosome), with a notable pattern at the X chromosome tip where H3K23me3 seems increased. This is potentially interesting and should be briefly commented on in the Results or Discussion, for example, whether this reflects compensatory activity of another HMT, changes in chromatin organization, or could be a technical artifact.

(3) Figure 3d suggests that some actively expressed genes can also display relatively high H3K23me3 levels, which complicates a simple model of H3K23me3 as exclusively repressive. If feasible, a limited additional analysis stratifying genes by both H3K23me3 and H3K9me3/H3K27me3 status might clarify whether these highly expressed, H3K23me3-marked genes differ in other chromatin features.

(4) The authors argue that SET-19 primarily affects H3K23me3 and not other canonical repressive marks, based largely on mass spectrometry. It would significantly strengthen the mechanistic conclusions if the authors could assess H3K9me3 and H3K27me3 profiles in set-

19 mutants, ideally by ChIP-seq or at least by focused ChIP-qPCR at a subset of loci that lose H3K23me3 and are derepressed at the RNA level. This would address whether H3K23me3 loss occurs independently of changes in other heterochromatin marks, or whether there is crosstalk.

https://doi.org/10.7554/eLife.111326.1.sa1

Author response:

> ***Public Reviews:***
>
> ***Reviewer #1 (Public review):***
>
> *Summary:*
>
> *The authors wanted to determine whether the set-19 gene, one of 38 SET-domain containing genes in C elegans, has a clear function in vivo with respect to lysine methylation. The question is not only whether it can modify this histone tail residue, but also what the impact of a loss of this locus is on the inheritance of repressive chromatin states.*
>
> *Strengths:*
>
> *The authors clearly achieved their goal, and it is convincingly shown that SET_19 is indeed a somatic cell histone methyltransferase with a striking specificity for H3K23. There is both recombinant protein work, quantitative mapping in vivo, of histone marks and transcriptional changes, and the authors rule out some other hypotheses that have been in the literature. Overall, this provides a compelling argument that SET-19 is indeed the major somatic cell HMT for this residue. Interestingly, the phenotypes are rather minimal, consistent with redundancy in the physiological roles of histone methylation, and redundancy as well in HMT function. For the most part, the data are not over-interpreted. The genetic alleles used, assuming they are confirmed, were revealing and well-documented.*

Thanks very much for the positive comments on our work.

The alleles used in this study were confirmed by PCR and Sanger sequencing, and the sequence information will be added in the revised manuscript.

> *Weaknesses:*
>
> *The major weaknesses are easily fixed. The major weaknesses mainly reflect a slight overstatement of certain data (claiming insignificance, when it is not clear how that was determined) and claiming a bit too much about SET-32, which was independently claimed to be an H3K23 HMT. Clearly, the two SET domain enzymes are not redundant, nor is the claim that SET-32 has no role in H3K23 methylation completely convincing. Especially in germline or embryonic conditions. Finally, the imaging is not of very high quality, nor are the images fully quantitated. These points can be easily remedied.*

Thanks very much for the comments.

We agree that some interpretations in the original manuscript were too strong, particularly regarding the negative results and the role of SET-32. Our *in vitro* assays show that SET-32 exhibits H3K23me1 activity and, at higher SAM concentrations, activity toward H3K23me2/3. These findings indicate that SET-32 does have a role in H3K23 methylation. SET-32 is expressed in germ cells, oocytes, and embryos. It is quite likely that redundancy of H3K23 methyltransferase activity exists in these tissues. In the revised manuscript, we will tone down the interpretations and expand the Discussion section to include this possibility. We

will also replace the relevant images with higher-quality versions and provide quantitative analyses for Figures 6a and 6b.

> ***Reviewer #2 (Public review):***
>
> *Summary:*
>
> *This manuscript identifies SET-19 as a somatic H3K23 methyltransferase in C. elegans, building on previous genetic evidence for a role of set-19 in H3K23me3 regulation. The authors combine quantitative mass spectrometry, western blotting, in vitro methyltransferase assays, ChIP-seq, and RNA-seq to show that loss of set-19 causes a strong reduction of H3K23me3, particularly in somatic tissues, and is associated with derepression of a subset of genes enriched for H3K23me3. They further conclude that SET-19 is dispensable for canonical feeding RNAi and for transgenerational or intergenerational inheritance of RNAi, distinguishing its function from other heterochromatin-associated methyltransferases such as SET-25, SET-32, and the H3K27 HMTs. Overall, the work adds an important piece to the H3K23 methylation pathway and tissue-specific chromatin regulation in C. elegans.*
>
> *Strengths:*
>
> *Very strong genetic and biochemical evidence for SET-19 as the major H3K23me3 HMT.*
>
> *The mass spectrometry and western blot data convincingly demonstrate a strong reduction of H3K23me3 in two independent set-19 alleles and rescue by GFP::SET-19, which is a major strength (Figure 1, including Figure 1f).*
>
> *The in vitro methyltransferase assays (Figure 2) showing robust H3K23me1/2/3 activity for SET-19 SET+CC and only modest H3K23me activity for SET-32, together with the SAM titration experiment in Figure 2C, are very informative and nicely support the conclusion that SET-19 is a high-activity H3K23 methyltransferase compared to SET-32.*
>
> *The ChIP-seq analysis is central to the conclusions that H3K23me3 is enriched on chromosome arms, co-localizes with H3K9me3/H3K27me3, and is strongly reduced in set-19 mutants.*

Thanks very much for the positive comments on our work.

> *Weaknesses:*
>
> *(1) The global reduction of H3K23me3 in Figure 3b,c and Figure S4c is convincing, but the correlation analysis between H3K23me3 loss and mRNA changes in Figure 3g could be strengthened. Currently, the analysis appears to focus on broad categories; it would be helpful to provide:*
>
> *Representative genome browser tracks (e.g., exemplary gene coverage plots) for several genes that show clear H3K23me3 peaks in wild type, reduction in set-19, and concomitant upregulation of mRNA levels, and for a few genes that retain H3K23me3 and do not change expression. This would make the link between chromatin changes and transcriptional output more concrete.*

Thanks very much for the suggestion.

To address this point, we will include representative genome browser tracks for selected genes in the revised manuscript. These examples will help better illustrate the relationship between H3K23me3 loss and mRNA expression changes.

> *(2) In Figure S4C, the authors note a pronounced reduction of H3K23me3 mainly on chromosome arms, but in the current data, it appears that the impact might be arm-*

> *specific (i.e., stronger reduction in one arm than the other in a chromosome), with a notable pattern at the X chromosome tip where H3K23me3 seems increased. This is potentially interesting and should be briefly commented on in the Results or Discussion, for example, whether this reflects compensatory activity of another HMT, changes in chromatin organization, or could be a technical artifact.*

Thanks very much for bringing up this point.

As shown in Figure S4C, the overall chromosomal distribution pattern of H3K23me3 is broadly similar between wild type and *set-19* mutants, with pronounced enrichment over one chromosomal arm, whereas the center and the opposite arm show relatively lower signal. In *set-19* mutants, this asymmetry becomes more pronounced, with a larger difference between the highly enriched arm and the lower-signal regions. This pattern is particularly evident on chromosomes I, II, V, and X. These observations suggest that the effect of *set-19* loss on H3K23me3 is not uniform across chromosomal regions.

Substantial H3K23me3 signal remains in specific regions in *set-19* mutants, suggesting that additional enzyme(s) also contribute to H3K23me3 methylation. For example, SET-19 appears to function predominantly in somatic tissues, yet the ChIP-seq assays were performed using whole animals, including the germline. Alternatively, there might be compensatory activity of another HMT. In the revised manuscript, we will state these points more explicitly in the Results section and discuss the residual and locally increased H3K23me3 signals.

> *(3) Figure 3d suggests that some actively expressed genes can also display relatively high H3K23me3 levels, which complicates a simple model of H3K23me3 as exclusively repressive. If feasible, a limited additional analysis stratifying genes by both H3K23me3 and H3K9me3/H3K27me3 status might clarify whether these highly expressed, H3K23me3 marked genes differ in other chromatin features.*

Thanks very much for the suggestion.

To address this point, we will perform additional stratified analyses of H3K23me3-marked genes according to their H3K9me3 and/or H3K27me3 status. We will also compare highly and weakly expressed H3K23me3-marked genes to examine whether they differ in other chromatin features, including H3K9me3, H3K27me3, and, if feasible, H3K4me3 and H3K36me3.

> *(4) The authors argue that SET-19 primarily affects H3K23me3 and not other canonical repressive marks, based largely on mass spectrometry. It would significantly strengthen the mechanistic conclusions if the authors could assess H3K9me3 and H3K27me3 profiles in set-19 mutants, ideally by ChIP-seq or at least by focused ChIP-qPCR at a subset of loci that lose H3K23me3 and are derepressed at the RNA level. This would address whether H3K23me3 loss occurs independently of changes in other heterochromatin marks, or whether there is crosstalk.*

Thanks very much for the suggestions.

As suggested, H3K9me3 and H3K27me3 ChIP-seq in wild-type and *set-19* mutants will be performed. We will compare their genome-wide distributions and identify loci with significantly altered H3K9me3 and/or H3K27me3 enrichment. These analyses should help clarify whether H3K23me3 loss occurs largely independently of H3K9me3/H3K27me3 changes or reflects potential crosstalk among these repressive chromatin marks. In addition, we will examine H3K9me3 and H3K27me3 enrichment at genes showing both H3K23me3 loss and increased mRNA expression in *set-19* mutants to assess whether derepression at these loci is accompanied by changes in other canonical repressive marks.

https://doi.org/10.7554/eLife.111326.1.sa0